University of Bergen

Department of Physics and Technology

Master Degree Project in
Measurement Science and Instrumentation

Hydrate Monitoring using Capacitive Sensors

ZAHRA BAYATI

June 2013

Abstract

Gas hydrates are of particular interest in petroleum industry since their formation during oil-production can be a major risk factor. Gas hydrates can block pipelines, interrupt production, and in worst case even cause bursting flow lines. There are a few strategies available to monitor the hydrocarbon flow in pipelines in order to give an early warning system against hydrate formation. A potential technique is to monitor changes in the dielectric properties of the flow, and relate these to hydrate formation. There is however a need for a dielectric measurement technique which can perform bulk permittivity measurements to detect gas hydrate formation. This is because gas hydrate formation is not always a homogenous process, and it can take place in the bulk phase of a multiphase flow. A potential technique for bulk permittivity measurements is based on capacitance measurement methods.

This thesis studies the feasibility of using the capacitance sensing technique to monitor the formation of gas hydrates. To achieve this goal, a non-intrusive capacitance measurement system prototype has been designed, constructed, and tested under varying operating conditions. The COMSOL Multiphysics software tool has been used to determine an appropriate sensor design configurations of a capacitance sensor prototype. The design configurations are subsequently utilized for the construction of an experimental capacitance sensor. Finally, the ability of the capacitance sensor to identify permittivity changes during gas hydrate formation is experimentally investigated. To do so, the temperature and capacitance of two hydrate-forming test-samples with different water fractions have been measured in the kHz frequency range. The measured capacitance data was then used to find the permittivity information of the sample using capacitance sensor calibration curves. By following the measured permittivity and temperature variations of the hydrate-forming samples as a function of time, it is shown that the information derived from the capacitance sensor can be an indication of different stages of hydrate generation and evolution, for instance, (i) the onset and completion of the hydrate generation, (ii) phase inversion in the hydrate forming sample, and (iii) the permittivity relaxation related

to the hydrate generation. This study verifies that permittivity measurements with these types of sensors can be used to monitor the generation of gas hydrates.

Although important information about formation of gas hydrates can be obtained from the measured permittivity, no industrial applications of the capacitance sensors in the field of gas hydrate characterization have been reported so far. In addition, correlating the measured changes in dielectric parameters to the gas hydrate formation requires more analytical work.

Acknowledgment

I am deeply grateful to several people for their assistance and support for the fulfillment of this thesis.

I would like to express my gratitude to my supervisor, senior scientist Kjetil Folgerø, for all his valuable guidance and advice throughout this work. I am most grateful for his comments and suggestions during the phase of the development and the writing of this thesis.

I wish to express sincere appreciation to my supervisor, associate professor Bjørn Tore Hjertaker, for his support, imminent encouragement and positive attitude. He has always been there for me to help with the project issues.

I am also grateful to my supervisor, professor Richard Thorn, for his helpful contributions and discussions throughout this work.

Following, I would like to thank professor Erling Asbjørn Hammer, for sharing his invaluable knowledge, and interesting and clarifying discussions in relation to the capacitance sensor issues.

Special thanks are extended to senior scientist Jan Kocbach and PhD student Kjetil Haukalid, for willingly sharing their experience and knowledge. Their generous advice on theoretical issues and the problems concerning COMSOL Multiphysics simulation are highly appreciated.

Lastly, I would like to thank my family and my friends, for all their love, moral support and encouragement, and my parents, for their unconditional love, support, and motivation throughout my education.

Finally, and undoubtedly most important, I want to thank my beloved husband Reza, whose faithful support made me determined to finish this work. I would like to express my deepest gratitude to him for standing right behind me with all his sensitivity, understanding and patience. This work would be impossible without his support and care.

This page is left intentionally blank.

List of Contents

List of Tables

List of Figures

This page is left intentionally blank.

List of Abbreviations

Symbols	Description
TI	Thermodynamic inhibitor
MEG	Mono ethylene glycol
KI	Kinetic inhibitor
THF	Tetrahydrofuran
C	Capacitance
Q	Charge
V	Electric potential
ε	Permittivity
ε_0	Permittivity of vacuum
ε_s	Static relative permittivity
ε_r	Relative permittivity
P	Polarization
A	Area between the two electrode plates
d	Distance between the two electrode plates
ε_∞	High frequency permittivity
ε*	Complex relative permittivity
ε'	Dielectric constant
ε''	Dielectric loss
f_d	Dispersion frequency
τ	Relaxation time
σ	Conductivity
E	Electric field
E_0	External electric field
E_i	Induce electric field
σ_0	Free charge density
σ_i	Induced charge density
ECT	Electrical capacitance tomography
C_m	Capacitance of mixture
R_m	Resistance of mixture
C_x	Measured capacitance
R_x	Measured resistance
ω	Excitation frequency
C_{pw}	Pipe-wall capacitance
σ_{oil}	Conductivity of oil
σ_w	Conductivity of water
ω_f	Critical frequency
FEM	Finite element method
D	Electric displacement
H	Magnetic field intensity
ρ	Electric charge density

B	Magnetic flux density
J	Current density
W_{stored}	Stored electric energy
R_1	Electrode radius
R_2	Outer pipe radius
R_3	Inner pipe radius
R_4	Screen radius
h	Pipe height
l	Electrode length
w	Electrode width
θ	Electrode arc angle
x_e	Mole fraction of ethanol in ethanol/water mixture
β	Water fraction
CP	Cyclopentane
E_{eff}	Effective permittivity of mixture
C_{meas}	Measured capacitance
C_{air}	Capacitance of air-filled capacitor

1. Introduction

1.1. Motivation

One of the solid deposits which may form in oil and gas production, transportation and processing facilities is the *gas hydrate*. Gas hydrates are ice like crystalline compounds formed by small gas molecules (such as methane, ethane or carbon dioxide) and water [1, 2]. They belong to a group of compounds called *clathrates* (for more details see Chapter 2).

Gas hydrate formation requires certain conditions such as low temperature combined with high pressure. These conditions can be met in an oil and gas production process which is usually a high pressure operation, combined with the low temperature at the seabed, where subsea production facilities are located. In addition, there is always an excess amount of water coming from an oil reservoir into the drilled wells along with hydrocarbons that are in the hydrate guest size range. Thus, the possibility of gas hydrate formation in oil and gas production facilities is very high.

As gas hydrates form, they can deposit on the pipe walls or agglomerate into large solid deposits which can eventually lead to pipeline blockage. Moreover, movement of hydrate plugs in the pipeline at high velocities can cause the pipeline to rupture or even blowouts or eruption of the plugs through pipeline bends. For these reasons, gas hydrate formation can lead to serious operational and safety concerns. Gas hydrate plugging up a pipeline may cost the gas industry in excess of approximately 1 million U.S. dollars each day due to production shut down [3], and once a hydrate plug has formed, it can take weeks or even months to dissociate its safely and may require complex operations such as pigging for plug removal [4].

The prevention of hydrates requires substantial investment, typically up to 10 to 15% of the production cost [5]. Therefore, from both an economic and operational safety perspective, there has been a considerable need to understand the mechanism of gas

hydrate formation in order to better manage and mitigate the hydrate formation risks in the petroleum production sector.

The main motivation for this thesis is the need for monitoring hydrate formation by means of a dielectric measurement instrument based on the capacitance method, and the prospect of being able to develop this instrument for on-line measurements. The reason for choosing the capacitive measurement method is that the formation of gas hydrates will give a change in the capacitance. Thus, the capacitance measurement can provide valuable information about the formation process of gas hydrates and it can be a potential technique for gas hydrates detection.

1.2. Background

Current industrial solutions for avoiding hydrate formation are mainly by thermodynamic means, i.e. maintaining the temperature and pressure at a safe level and removing water, or by injecting 10-50% volume of *Thermodynamic Inhibitors (TI)* such as mono ethylene glycol (MEG) to the fluids [6]. In addition to thermodynamic inhibitors, new methods such as *kinetic inhibitors (KI)* and *anti agglomerants* have been developed in the past decade to prevent hydrate crystal growth and agglomeration, respectively. In this method, polymers and surfactants are added to the flow in the pipelines forming water-in-oil emulsions or microemulsions. Consequently, gas hydrates are only formed in the small water droplets, and large plug deposition will be prevented [7]. However, to minimize the risk of hydrate formation, it is common practice to use an excess amount of inhibitor. An excessive dosage of inhibitor results in negative environmental impacts and unwanted extra cost. For this reason, the need to minimize the amount of inhibitors is another motivation for further studies to understand the mechanisms of gas hydrate formation.

As mentioned, when gas hydrates form, free water molecules form clathrate structures. Since the dielectric properties of gas hydrates are different from water, bulk permittivity measurement can be an appropriate way of monitoring the formation of gas hydrates.

Dielectric property (permittivity) measurement methods range from low frequency capacitive methods to high frequency microwave techniques. Permittivity measurement methods are generally divided into single and broadband frequency methods. Although single frequency methods ensure high accuracy permittivity measurements, they are rather time consuming methods. In contrast, broad band methods provide quicker permittivity measurements over a wide frequency range, but they are less accurate.

At low frequencies (i.e. below approximately 10 MHz), parallel plate and coaxial capacitors are commonly used to estimate the permittivity of a sample by placing the sample in the capacitor and then measuring the admittance of the cell with an impedance bridge [8]. At radio and microwave frequencies below approximately 10 GHz, coaxial measurement cells are mainly used by calculating the permittivity of a sample from the measured transmission and/or reflection coefficient of the cell. High accuracy permittivity measurements at microwave frequencies are obtained by single frequency waveguide methods such as the variable length waveguide method and the cavity resonator technique [9-11].

Jacobsen *et al.* [12] have shown that the formation of gas hydrates in emulsions can be monitored by means of dielectric spectroscopy with a modified open-ended coaxial cell. The drawback of their measurement system was that the sensor was intrusive. Furthermore, the coaxial cells have a very low measurement volume, which means that only the permittivity of materials very close to the end of the probes affect the measurements. This makes these cells suitable only for measurements on thin liquid levels [13]. On the other hand, the measurements are not capable of representing the bulk permittivity of sample under test. Jakobsen and Folgerø [14] studied the applicability of non-intrusive open-ended coaxial probes for permittivity measurements of gas hydrate formation. Their sensor represented a better quality of the measured dielectric spectrum at high frequencies than those acquired by Jacobsen *et al.* [12]. However, the measurement

volume of open-ended probes is low and they provide a small sensitivity depth. Because gas hydrate formation is not always a homogeneous process, and it takes place in a form of hydrate clusters, local measurements performed by open-ended probes may not give enough information about the bulk permittivity of the emulsion.

Therefore, there is a need to design a non-intrusive measurement system with high sensitivity. Suggested measurement systems for this purpose are parallel plate capacitors at low frequencies, large open ended probes at intermediate frequencies and waveguides at high frequencies [13, 15].

1.3. Objectives

The objective of this thesis is to design and test a non-intrusive prototype measurement system based on a capacitance sensing technique in order to monitor the formation of gas hydrates. The capacitance sensor will then be used to determine if bulk permittivity measurements at a low frequency are accurate and sensitive enough to monitor gas hydrate formation in water/oil emulsions.

In this thesis, a capacitance sensor model is implemented using the COMSOL multiphysics software to optimize the capacitance system parameters and to determine the most appropriate electrode configuration for monitoring and detection of gas hydrate formation. This is done for a range of operating conditions including operating frequency and water content of the hydrate forming emulsion.

An experimental setup is established for measuring the capacitance of an emulsion during gas hydrate formation. The capacitance of hydrate formation in emulsions is measured for various water fractions and operating frequencies. In order to calibrate the system and determine the sensitivity and accuracy of the measurement setup, the capacitance of known reference liquids is measured.

1.4. Outline

The thesis begins with a brief introduction to gas hydrate structure, the theory of capacitors, measurement techniques, current applications, and challenges facing the capacitive methods in Chapter 2.

Chapter 3 provides a numerical and finite element analysis of a specific capacitance electrode configuration using COMSOL Multiphysics in order to identify the optimum design of the electrodes for permittivity measurements of gas hydrate formation.

In Chapter 4, the elements of the measurement instruments used in monitoring formation of gas hydrates as well as a description of the experimental procedure are presented.

Chapter 5 presents experimental results obtained from the capacitance sensor prototype. In this chapter the ability of the sensor to identify permittivity changes during formation of gas hydrates is experimentally investigated.

Chapter 6 summarizes and concludes the main achievements of the thesis, and suggestions for future work will be given in Chapter 7.

2. Background Theory

As discussed in Chapter 1, the main objective of this thesis is to monitor gas hydrate formation by means of capacitance sensors. To achieve this goal, an insight into the fundamentals of gas hydrate formation phenomenon and capacitance sensors is required. Therefore, this chapter presents a brief overview of these two subjects in Section 2.1 and Section 2.2, respectively.

2.1. Gas hydrate

In this Section, an introduction to structures, general attributes and challenges for gas hydrates formation is presented.

2.1.1. Chemical structures of hydrates

Gas hydrates are a large subgroup of clathrate[1] hydrates formed mostly under relatively high pressure of 10-30 MPa and low temperatures from deep negative up to 20-25 °C. However, the typical stability temperatures of gas hydrates are generally below 15-20 °C [5]. In the gas hydrate structure, a water crystal cage is built by the hydrogen-bonded water molecules (host molecules), whereas smaller molecules (guest molecules) are entrapped in the water cages stabilizing the lattice structure [2]. Depending on the nature and size of the guest molecules, hydrates can form one of the three repeating crystal structures [1]: structure-I, structure-II, and structure-H.

[1] A clathrate compound is a chemical substance made of a lattice which traps or contains other molecules.

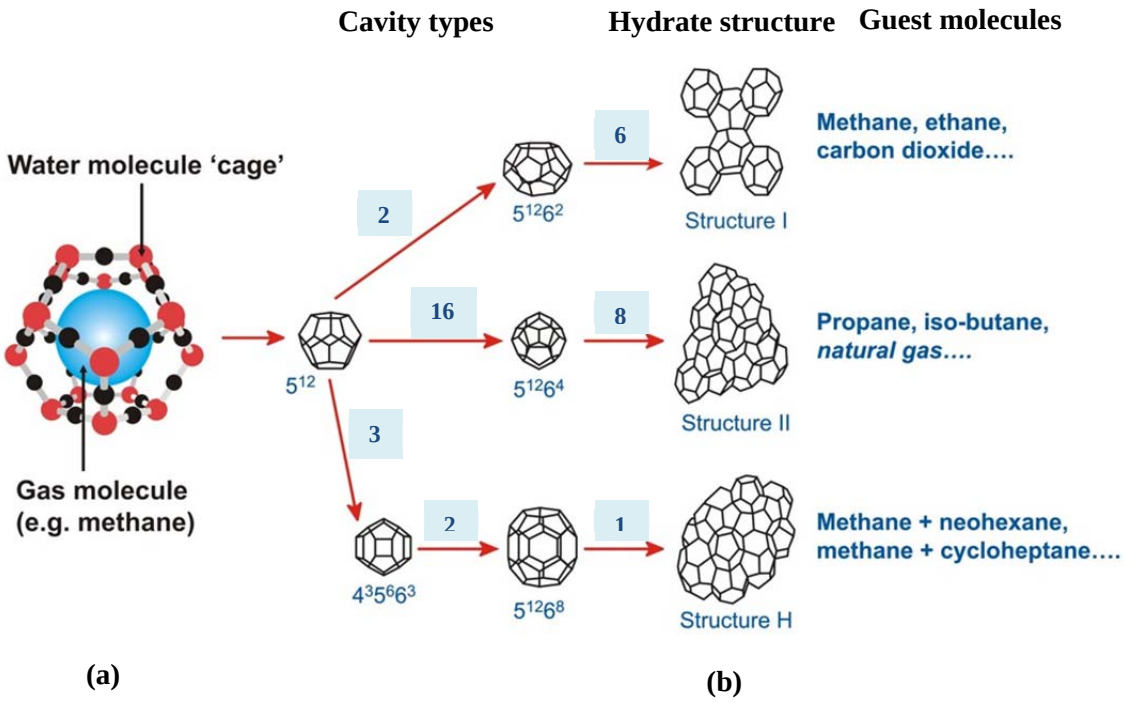

Figure 2.1: Figure taken from [7]: (a) Water molecules form a cage-like structure and guest molecules (e.g. methane) are contained in it. (b) The three common hydrate unit crystal structures. Nomenclature: $5^{12}6^2$ indicates a water cage composed of 12 pentagonal and 2 hexagonal faces. The numbers in squares indicate the number of cage types. For instance, the structure I unit crystal is composed of two 5^{12} cages and six $5^{12}6^2$ cages.

Light weight gas molecules of a size less than 0.6 nm form the structure-I hydrate. Methane, ethane, carbon dioxide and hydrogen sulfide are examples of guest molecules which can form structure-I hydrate. Note that the combination of methane and ethane can form structure-II formed from larger molecules with sizes in the interval from 0.6 and 0.7 nm. These hydrates can be formed by propane, isobutane, etc. Gases with a molecular size between 0.7 and 0.9 nm can form structure-H. Hydrocarbons such as cyclopentane and Tetrahydrofuran (THF) are examples of structure-H hydrates [16]. Figure 2.1 shows these three common unit crystal structures.

2.1.2. Kinetics of gas hydrate formation

The hydrate formation process is a stochastic phenomenon and it is analogous to the crystallization process [17]. This process can be divided into two stages: hydrate

nucleation and hydrate growth. The hydrate nucleation is a microscopic stochastic phenomenon where the gas-water clusters (nuclei) grow and disperse until some nuclei grow to critical sized stable hydrate nuclei. Hydrate nucleation may occur spontaneously, or it may be induced around impurities. After the nuclei are reached to a critical size, the hydrate growth process begins. This process refers to the growth of stable hydrate nuclei as solid hydrates.

The growth of gas hydrates are dependent on many factors such as the amount of the hydrate former substance (guest molecules) and how the hydrate former substance is dissolved in water. Therefore, the hydrate growth period may differ substantially according to the thermodynamic and chemical conditions of hydrate formation. The hydrate growth is an exothermic process. Therefore, the increase, decrease and stabilization of the temperature during the hydrate formation provide the information of kinetics and the thermodynamics of this process. Nevertheless, there is still little knowledge of the dynamic process in hydrate growth during the formation process.

2.1.3. Physical properties and implications

Physical properties of hydrates are determining factors for their roles that they play in both industry and the environment. Hydrates have a solid and non-flowing nature, and their densities are higher than typical fluid hydrocarbons. Gas hydrates stabilize under certain pressure and temperature conditions which can be met in deep seabed where oil and gas pipelines are installed. In addition, in oil and gas wells there is always undesired water along with hydrocarbons in the hydrate guest size, and this may lead to formation of gas hydrates inside the pipelines.

The formation of gas hydrates inside the pipelines is an undesired event from one perspective, because it may block or hinder the flow of oil and gas. The petroleum industry tends to devise practical implications for flow assurance in oil and gas transportation pipelines and the safety thereof. On the other hand, the fact that hydrates concentrate their guest molecules results in a number of potential useful applications for hydrates as well; e.g. energy can be recovered from in situ hydrates [18]; hydrates can be

used for natural gas storage and transportation [19-21]; hydrates may be a factor in climate change [22, 23]; it can be employed for water purification [24] and evaluation of water desalination [25].

2.2. Capacitance sensors

Capacitive sensors are widely used for a large variety of measurement applications. They can be used to sense a variety of physical variables directly e.g. motion, electric field, chemical composition, and many other variables indirectly such as pressure, acceleration, fluid level, and fluid composition, which relate to the motion or the dielectric constant [26].

2.2.1. Fundamental principles

A capacitor is an electronic component which can store electric potential energy and charge. A capacitor fundamentally consists of two electrical conductive electrodes isolated from each other by a surrounding medium called a dielectric. By applying a potential difference across the two electrodes, the capacitor is charged and both electrodes carry equal but opposite amount of charges on the electrodes. The difference in the electric potential V across the electrodes is proportional to the charge Q accumulated on the capacitor, while the ratio of Q over V is a constant value called the capacitance C which is measured in Farad [F]:

$$C \equiv \frac{Q}{V} \tag{1}$$

By definition, the capacitance quantity will be always positive, and since the potential difference increases with an increase in the stored charge, the Q/V ratio will be constant for a given capacitor. In general form, the capacitance value depends on the electrode's geometrical arrangement, the distance between the electrodes and the permittivity of the insulating material separating the charged electrodes (called the dielectric material).

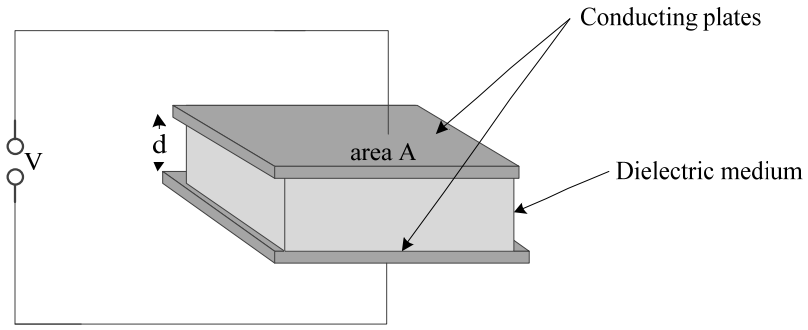

Figure 2.2: A parallel plate capacitor.

The simplest form of a capacitor consists of two parallel metal plates across which a potential difference is applied, as shown in Figure 2.2. For simplicity, in this section, the basis of the capacitance measurement principle is explained using the parallel plate as an example. The capacitance between two oppositely placed electrodes is given by the expression [27]:

$$C = \varepsilon \frac{A}{d} \tag{2}$$

Where A is the overlapping area between the two conducting plates, d is the distance between the conducting plates, ε is the permittivity of the surrounding medium. Permittivity ε is calculated by:

$$\varepsilon = \varepsilon_0 \varepsilon_r \tag{3}$$

where ε_0 is the permittivity of free space (vacuum) of magnitude 8.854×10^{-12} F/m and ε_r is the relative permittivity (or dielectric constant) of the insulating dielectric material.

2.2.2. Dielectrics

The term dielectric is usually used to signify materials with low conductivity and high insulation characteristics. When a dielectric material is inserted between the conducting plates of a capacitor, it increases the capacitance value by decreasing the potential difference by a dimensionless factor ε_r, called the dielectric constant. Since the potential difference between the plates is equal to the product of the electric field and the conducting plates separation:

$$\Delta V = E.d \tag{4}$$

the electric field is also reduced by the factor ε_r. Thus, if $\vec{E}_0$ is the electric field with no dielectric material, and $\vec{E}$ is the field in the presence of a dielectric, dielectrics cause the electric field inside the capacitor to be reduced.:

$$\vec{E} = \frac{\vec{E}_0}{\varepsilon_r} \tag{5}$$

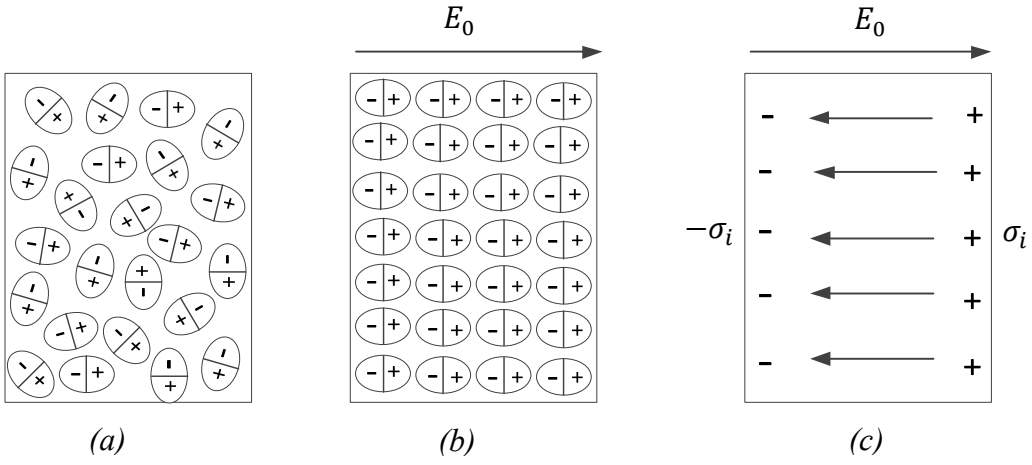

Figure 2.3: Polarization of the dipoles by external electric field E_0.

This is because the molecules of a dielectric material can get polarized. Dielectrics can be subdivided into two types of polar and nonpolar. The molecules of a polar dielectric material possess a permanent electric dipole in the absence of an electric field, e.g. water,

whereas permanent electric dipoles are not present in a nonpolar dielectric material. In the absence of an electric field, the dipoles are randomly orientated, as shown in Figure 2.3 (a). When the dielectric material is placed in an external electric field, as shown in Figure 2.3 (b), the dipoles get partially or fully aligned in the direction of the electrical field. Consequently, induced charges are formed on the two sides of the dielectric, dependent on whether the dielectric consists of polar or nonpolar molecules. The dipoles align themselves in a way that an induced electric field is set up inside the dielectric opposite to the direction of the external field. The induced electric field produced by the polarization will therefore reduce the original electric field. The net result of the alignment of the individual dipoles is the formation of equal positive and negative surface charge densities σ_i on either sides of the dielectric material, as shown in Figure 2.3 (c).

Thus, the net electric field $\vec{E}$ in the dielectric has a magnitude given by Equation (6) where $\vec{E}_i$ and $\vec{E}_0$ are the induced and external electric fields, respectively:

$$\vec{E} = \vec{E}_0 - \vec{E}_i \tag{6}$$

The relationship between the external field $\vec{E}_0$ and the free charge density σ_0 on the conductors of a parallel plate capacitor is given by the relation:

$$\vec{E}_0 = \frac{\sigma_0}{\varepsilon_0} \tag{7}$$

The induced electric field in the dielectric is related to the induced charge density σ_i through:

$$\vec{E}_i = \frac{\sigma_i}{\varepsilon_0} \tag{8}$$

Therefore, the net electric field inside the capacitor decreases to:

$$\vec{E} = \frac{\vec{E}_0}{\varepsilon_r} = \frac{\sigma_0}{\varepsilon_r . \varepsilon_0} \tag{9}$$

This drop in the net electric field can also be considered as a decrease in the charge density:

$$\frac{\sigma_0}{\varepsilon_r.\varepsilon_0} = \frac{\sigma_0}{\varepsilon_0} - \frac{\sigma_i}{\varepsilon_0} \tag{10}$$

$$P = \sigma_i = (\frac{\varepsilon_r - 1}{\varepsilon_r})\sigma_0 \tag{11}$$

where P is the electrical polarization.

One aspect of the electric field that is defined solely by the free charge densities is called the electric displacement D:

$$D = \varepsilon_r.\varepsilon_0.E = \varepsilon_0.E + P \tag{12}$$

When the frequency of external electric field is increased, the dipoles are not able to align themselves with the electric field. At sufficiently high frequencies, the dipoles do not contribute to the polarization any more leading to a gradual decrease in the permittivity (permittivity dispersion) from low-frequency (static frequency) $\varepsilon_r = \varepsilon_s$ to high-frequency $\varepsilon_r = \varepsilon_\infty$. This dispersion is characterized by a phase difference between the external electric field and the displacement vector. Therefore, the ratio of displacement to the electric field becomes a complex quantity:

$$\frac{D}{E} = \varepsilon^*\varepsilon_0 = (\varepsilon' - j\varepsilon'')\varepsilon_0 \tag{13}$$

where ε^* is the complex relative permittivity, and ε' and ε'' are the dielectric constant and dielectric loss, respectively. The presence of the phase difference between the electric displacement and the electric field causes the absorption of energy by the system. When the dielectric loss ε'', and thus, the phase difference is zero, the absorbed energy becomes zero as well. The frequency, where the dielectric loss ε'' is at its maximum level, is called the dispersion or relaxation frequency f_d. The relaxation time is then defined as:

$$\tau = \frac{1}{2\pi f_d} \tag{14}$$

In the complex materials, several relaxation processes can take place. These relaxation processes can be described by the empirical models such as Cole-Cole [28] and Debye

[29]. Figure 2.4 shows the dielectric parameters, and the difference between a Cole-Cole and Debye dispersion profile.

When considering a gas hydrate forming flow, three relaxation processes occur in the dielectric spectrum of the gas hydrate formation process [12]. The first relaxation process occurs in the low frequency region (kHz frequency range), and it is due to the dispersion of gas hydrates. Other relaxation processes occurring at high frequencies are caused by the polarization of the conductive water droplets in the flow. Therefore, by measuring the frequency dependent permittivity, valuable information about the changes in the mixture system and the formation of gas hydrates can be obtained.

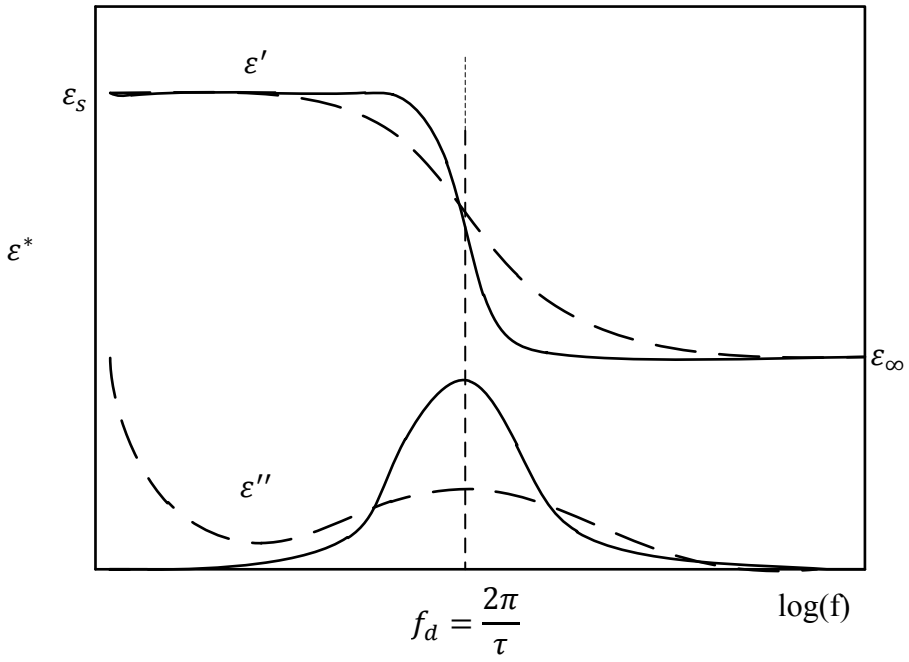

Figure 2.4: Dielectric relaxation process due to Debye model (solid line) and Cole-Cole model (dashed line) [13].

In Figure 2.5, a model spectrum of a water/oil emulsion with gas hydrates is shown [13]. The low frequency dispersion around 100 kHz is the dielectric relaxation of gas hydrates. The static permittivity value of the gas hydrate is equal to $\varepsilon_s = 58.0$.

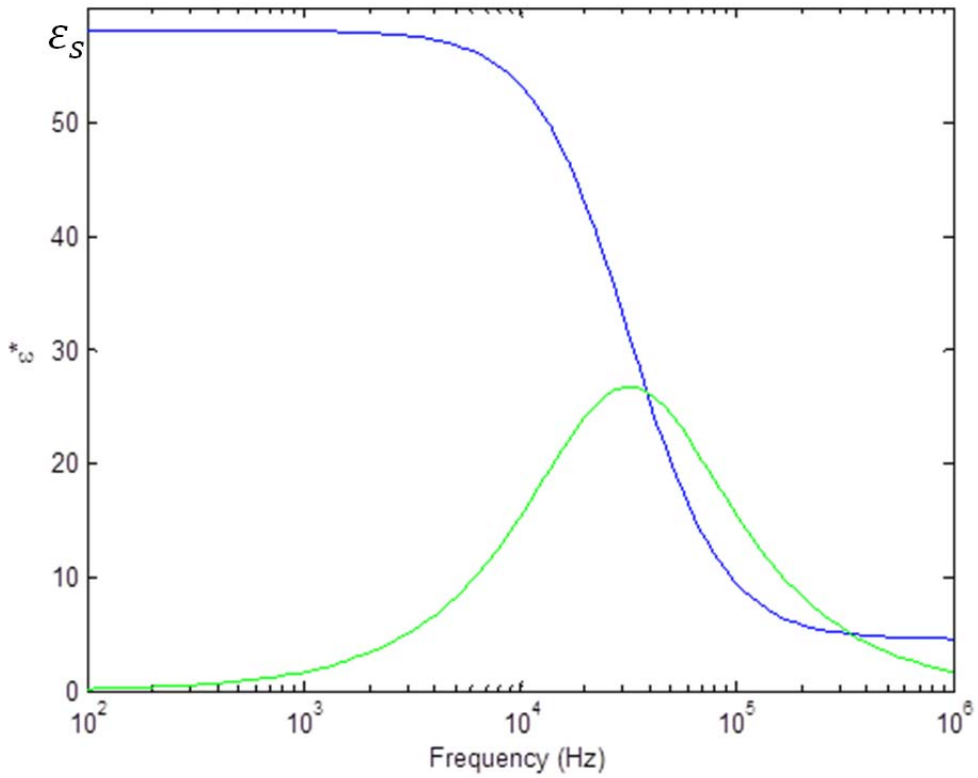

Figure 2.5: A Model spectrum of an emulsion with gas hydrates [13].

2.2.3. Applications

Capacitive techniques electronically measure the capacitance between two or more conductors, and have been applied to solve many different types of sensing and measurement problems [26]. Capacitive touchscreen based on pressure sensing [30] is one of the applications most related to people's life. Furthermore, capacitive techniques have been employed in many areas such as micrometer development [31], proximity and position sensing displacement measurement [32, 33] and materials characterization [34-37].

A practical application of the capacitive technique is in the field of material dielectric property characterization called dielectrometry, which yields the complex permittivity of a test material by means of a capacitance sensor. Interdigital dielectrometry sensors, with increased effective length and output capacitance between the electrodes have been used

for dielectrometry measurements due to their interdigital structure. The interdigital dielectrometry sensors have been applied in many fields such as material property monitoring, humidity and moisture sensing, electrical insulation properties sensing, monitoring of curing processes, chemical sensing, biosensing, etc [35, 36, 38-40].

Apart from interdigital dielectrometry sensors, other sensor configurations have been used for defect characterization, sensing moisture content, temperature, aging process, delamination, and inhomogeneities in dielectric materials. For instance, rectangular capacitance sensors have been used to detect specific surface features in conductive materials and ultrastructural features in dielectrics [41, 42]. In recent years cylindrical geometry quasistatic dielectrometry sensors have been developed to measure the permittivity of a dielectric plate [43]. Furthermore, rectangular coplanar capacitance sensors with high sensitivity have been developed for detection of water intrusion in composite structures [44] based on the fact that the presence of defects, for instance water, cause the dielectric characteristics in composite structures to be changed, leading to variations in the measured capacitance of the sensor. On the basis of a similar principle, rectangular coplanar capacitance sensors have been applied for detecting damage in laminated composite plates [45]. In addition, these techniques have even been used to monitor the tissue cultures and thickness of biofilms [46].

Electrical capacitance tomography (ECT) is another application of capacitance techniques that is employed for imaging cross sections of industrial processes containing dielectric materials [47]. The principle is that the test piece permittivity distribution and hence the material distribution over a cross section can be determined through image reconstruction. An application for ECT is identification of the flow pattern in oil and gas pipelines [48, 49].

Capacitance measurement techniques have also been widely investigated in the oil and gas industry to measure the distance, liquid level, speed and phase percentage of the multiphase flow in pipelines [50-53]. Capacitance sensors have been utilized in measuring the water content of crude oil since these sensors are sensitive to the existence of water due to its high permittivity [54-56]. So far, capacitance sensors have been only used for

homogeneous mixtures of water and oil due to the dependence of this technique on the distribution of the components in the mixture (flow regime) being monitored. For example, the calibration curve required for an annular flow would be different from that required for a bubble flow. It is, however, possible to deal with the flow regime dependency by various approaches. For example, if the sensor is installed on a specific location of the pipeline, e.g. after a bend, natural mixing of the flow produces a homogenous flow regime [57]. Employing helical shaped surface plate electrodes based on 180° twisted electrostatic field or rotating electric fields is an alternative approach to reduce the effect of flow regime dependency [58-60]. Another approach is to use multiple electrodes with sensitivity to different regions of the cross-section, and through that correct for flow regime changes [61].

2.2.4. Challenges

Capacitance sensor technology is widely used in the industry as it is inherently simple, robust, low cost, and has a faster dynamic response than many other types of sensors. In addition, accurate electronics for the capacitance sensors are currently available, and they are noise immune. However, capacitance techniques suffer from two important limitations: they are flow regime dependent and cannot be used over the full component fraction range.

If capacitance techniques are used for component fraction measurement, then the calibration of a capacitance component fraction meter is dependent on the flow regime of the flow being monitored. Therefore, these techniques cannot be used in applications where the flow regime is unknown or unstable. Nonetheless, even if the capacitance technique is flow regime dependent, it can still be used for the measurement of homogeneously mixed flows.

The other limitation which capacitance techniques face is that they cannot be used over the full component fraction range of an oil/water mixture. This implies that the capacitance sensor domain is insensitive to conducting liquids between the electrodes at

low excitation frequencies. Consequently, in order to conduct a capacitance measurement, it is generally required to use a non-conducting substance or liquid in the measurement volume. For instance, once the water emerges as the continuous phase in the oil and gas pipes, the electrical field inside the sensor becomes short circuited by the conducting ions in the water, rendering the capacitance sensor insensitive to the measured parameter. The short circuiting occurs at excitation frequencies below approximately 1 GHz. To have a better understanding of how this occurs, it is useful to model the capacitance sensor as an equivalent circuit as shown in Figure 2.6 [59]. In this figure, it is assumed that the capacitance sensor is formed from two electrodes which are curved to fit the outer pipe diameter of an insulated test section in which a mixture is flowing. The mixture is assumed to be an oil/water mixture with the oil as its continuous phase, and it can be modeled as a capacitance C_m (of pure imaginary impedance $1/j\omega C$) and a resistance R_m (of real impedance R) in parallel. C_{pw1}, and C_{pw2} represent the resultant pipe wall capacitances. Using this equivalent circuit for the sensor, the measured capacitance and equivalent parallel resistance will be [59]:

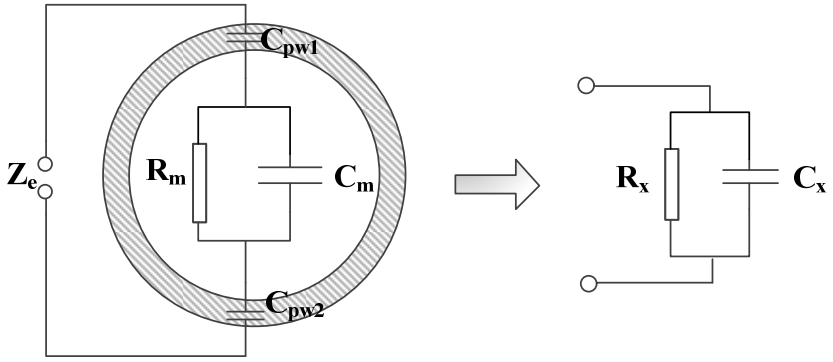

Figure 2.6: Equivalent circuit diagram of a capacitance sensor.

$$C_x = \frac{\{1 + \omega^2 R_m^2 C_m (C_m + C_{pw})\} C_{pw}}{1 + \omega^2 R_m^2 (C_m + C_{pw})^2} \tag{15}$$

$$R_x = \frac{1 + \omega^2 R_m^2 (C_m + C_{pw})^2}{\omega^2 R_m {C_{pw}}^2} \tag{16}$$

Here, $\omega = 2\pi f$ where f is the excitation frequency of the capacitance sensor and $C_{pw} = \frac{1}{2} C_{pw1} = \frac{1}{2} C_{pw2}$.

We can see from Equation (15) that the effective capacitance C_x is dependent both on the excitation frequency ω and on the resistance $R_m$of the mixture. Equation (15) also shows that the sensitivity of the sensor will increase with increasing electrode/bulk capacitance (C_{pw}) but decrease with decreasing bulk resistance R_m. In addition, in practical applications, Equation (15) is always fulfilled, and a typical behavior shown in Figure 2.7 is generally anticipated. As can be seen from this figure, for a well-mixed mixture of North Sea crude oil and water, a transition where the oil/water mixture shifts from oil continuous to being water continuous i.e., to the percolation point will occur at 78-80% water fraction.

In general, a homogeneous water/oil mixture is typically oil-continuous up to water fractions of 40% - 80%. The appearance of the percolation point will be dependent on many factors including the conductivity, i.e. the salinity of the flowing mixture, temperature, pressure, degree of mixing and the content of hydrocarbon components, e.g. 78-80% for typical North Sea crude oil [59].

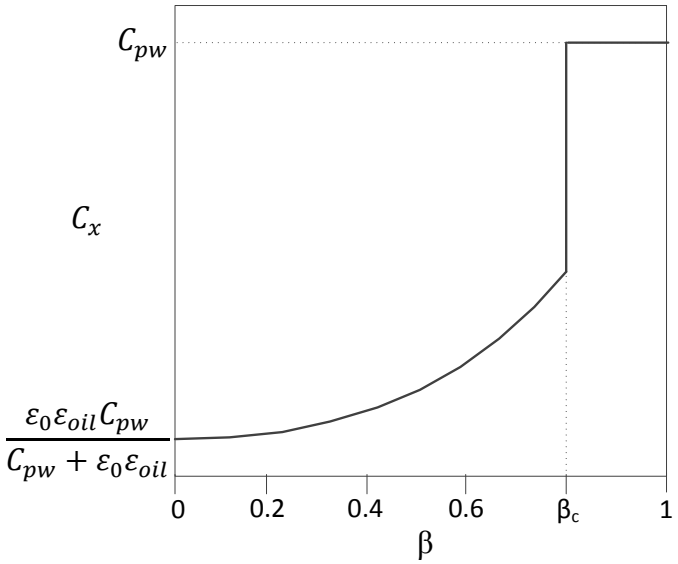

Figure 2.7: Effective capacitance per unit length of a surface plate capacitance sensor as a function of the water fraction β of a well-mixed mixture of North Sea crude oil and water [59].

We have so far assumed that the oil is the continuous phase in the oil/water mixture. If the water is the continuous component in the oil/water mixture, and the conductivity of the water is much larger than the conductivity of the oil $\sigma_w \gg \sigma_{oil}$, the current through the two elements of the equivalent circuit in Figure 2.6 will be equal when:

$$\frac{1}{\omega_c C_m} = R_m \;\rightarrow\; \omega_c = 2\pi f_c = \frac{1}{R_m C_m} \tag{17}$$

The mixture can be modeled as a slab of cross section area A and length L, such that:

$$R_m = \frac{\rho L}{A} = \frac{L}{\sigma_w A} \tag{18}$$

$$C_m = \frac{\varepsilon_w A}{L} \tag{19}$$

which means that:

$$\omega_c = \frac{1}{R_m C_m} = \frac{\sigma_w}{\varepsilon_w} \tag{20}$$

where ω_c is the critical frequency.

If the capacitance sensor excitation frequency is significantly lower than the critical frequency ω_c, i.e., $\omega_c \ll \frac{\sigma_w}{\varepsilon_w}$, a short circuiting effect will occur caused by the conductive water. When this happens, the only contribution to the capacitance measurement of the sensor will be solely the pipe wall capacitances $C_{pw1}$and C_{pw2}, and thus a constant value is measured even if the water volume fraction β varies (See Figure 2.7).

The conductivity of the sea water from North is approximately 5 S/m. Assuming that the relative permittivity of the same component is 80, we have:

$$f_c = \frac{\sigma_w}{2\pi\varepsilon_0\varepsilon_w} = \frac{5}{2\pi \times 8.85 \times 10^{-12} \times 80} = 1.12 \times 10^9\ Hz = 1.12\ GHz \qquad (21)$$

This means that when the oil/water mixture is water continuous, we have to operate at frequencies larger than approximately 1 GHz, which is not feasible for practical systems. For instance, a 100 kHz capacitance sensor will be insensitive to measurements of the oil/water mixture beyond the percolation point. Intrusive capacitance electrodes can fail to function before that point since local water collections will act as short circuiting paths between the electrodes. The issues relating to water continuous phase for the capacitance sensors can be problematic in horizontal pipe flows, since the water and the oil components tend to become separated due to the gravitational forces acting on the flowing liquid. Therefore, the capacitance sensors may become short circuited for only a few percent of water.

It can be concluded from this section that the capacitance sensor system can only measure the water fractions in oil up until the percolation point. It implies that the technique can sometimes be used for mixtures with water fractions of up to 80% (Figure 2.7). However, as mentioned before, the point at which a flow will shift from an oil or gas continuous to water continuous mixture is not stable. Adding corrosion inhibitors to the flow can even cause problems since they will lower the water fraction at which a flow becomes water continuous.

3. Design, Optimization and Construction of the Capacitive Sensor

3.1. Computer modeling of the capacitive sensor

Computer modeling can be used as an efficient way to test the functionality of a device under various operating conditions. Building a prototype can be costly and also take a long time. Computer models can be a cost effective alternative for determining if a device will function as predicted in theory. It is also possible to evaluate many different designs by modeling them in order to find the most appropriate design prior to building the device.

In this thesis, computer modeling is used in order to find an optimized capacitance sensor configuration for reliable identification of the gas hydrate formation. This will be determined by investigating the different sensor parameters including electrode position, electrode dimensions, and pipe configuration.

In this thesis, the design criteria of the capacitance sensor for identification of the gas hydrate formation can be defined as follows:

- The capacitance sensor should perform high sensitivity measurements where a small change in the dielectric material (gas hydrate formation in emulsions) leads to a large change in the measured parameter (capacitance).
- For a mixture of water and oil, the capacitance sensor should be applicable to measuring the permittivity over the whole range of 0-100% water.
- The capacitance sensor should be able to measure the bulk permittivity of the dielectric material (gas hydrate).

In this chapter, first, the Finite Element method (FEM) for modeling the capacitive measurement system is described in Sections 3.2 and 3.3. Then, the implementation of a

capacitive sensor by COMSOL Multiphysics simulation tool is presented in Section 3.4. This implementation is used to determine an appropriate sensor configuration design described in Section 3.5. In order to verify the implemented capacitance sensor model, an experimental setup of the sensor configuration is constructed. The construction details are presented in Section 3.6. Finally, the experimental setup is used to verify the implemented model in Section 3.7.

3.2. The finite element method

In this thesis the capacitive measurement sensor consists of two curved electrode plates which are mounted on the external wall of a cylindrical pipe (see Figure 3.1). The boundary conditions are such that one electrode is at zero potential, whereas the other electrode is kept at a non-zero potential. The electric potential distribution at any point between the two electrodes is governed by Laplace's equation [62]:

$$\nabla^2 V = \frac{\partial^2 V}{\partial x^2} + \frac{\partial^2 V}{\partial y^2} + \frac{\partial^2 V}{\partial z^2} = 0 \tag{22}$$

Solving the above equation for this capacitive sensor geometry and its boundary conditions is not simple, and in practice it is calculated numerically. For this reason, applying a numerical technique, for instance the Finite Element Method (FEM), will be an appropriate way to perform the calculations and thereby to find the electric field distribution.

The Finite Element Method (FEM) approximates solutions to the partial differential equations by dividing a complicated model into a number of smaller model elements, solving the partial differential equations for these smaller model elements, and finally integrating the solutions of these [63].

FEM simulations can be implemented using various software tools such as COMSOL Multiphysics [64] which will be used for finite element analysis in this thesis. COMSOL Multiphysics is an interactive physics solver and simulation software that performs the

modeling and simulation of any physical phenomena in a way that is quite simple to implement [65].

3.3. Governing equations

The challenge of electromagnetic analysis on a macroscopic level is that of solving Maxwell's equations subject to certain boundary conditions. The equations can be formulated in either differential or integral form. Since FEM can handle differential equations, the differential form of Maxwell's equations is as follows:

$$\nabla \times H = J + \frac{\partial D}{\partial t} \tag{23}$$

$$\nabla \times E = -\frac{\partial B}{\partial t} \tag{24}$$

$$\nabla . D = \rho \tag{25}$$

$$\nabla . B = 0 \tag{26}$$

The first two equations are referred to as Maxwell-Ampère's law and Faraday's law. Equation (25) and (26) are two forms of Gauss' law: electric and magnetic, respectively. The respective quantities are: Electric field intensity E $[V/m]$, electric displacement or electric flux density D $[C\ /\ m^2]$, magnetic field intensity H $[A/m]$, magnetic flux density B $[T]$, electric charge density ρ $[C]$ and current density J $[A\ /\ m^2]$ [66].

The equations governing the capacitive sensor model are based on the following assumptions [67]:

1. The material inside the capacitive measurement sensor is assumed to be linear and isotropic:

$$J = \sigma E \tag{27}$$

$$D = \varepsilon_0 \varepsilon_r E = \varepsilon E \tag{28}$$

2. It is also assumed that the magnetic flux density can be ignored and hence:

$$\nabla \times E = 0 \tag{29}$$

By considering these initial assumptions, the electric form of Gauss' law can be written as:

$$\rho = \nabla . D = \varepsilon_0 \varepsilon_r \nabla . E \tag{30}$$

Knowing that the electric field intensity can be written as the gradient of a scalar potential $E = -\nabla V$, where V is the electrical potential distribution, the equation becomes:

$$\rho = \nabla . D = \epsilon_0 \epsilon_r \nabla . E = -\epsilon_0 \epsilon_r \nabla . \nabla V = -\epsilon_0 \epsilon_r \nabla^2 V \tag{31}$$

This is called Poisson's equation [68]:

$$-\frac{\rho}{\epsilon_0 \epsilon_r} = \nabla^2 V \tag{32}$$

Poisson's equation is what needs to be solved when the Electrostatics (es) interface of the AC/DC module is selected in COMSOL Multiphysics.

When there is a dielectric material inside the sensing region of the capacitive sensor, the electric charge density is zero $\rho = 0$, and Poisson's equation reduces to Laplace's equation:

$$\nabla^2 V = 0 \tag{33}$$

The COMSOL Multiphysics simulation provides an approximation to the potential distribution V within the sensor at a finite number of points corresponding to the nodes of the tetrahedral mesh that is normally used in the finite element method [69].

In this way, the potential distribution within the sensor and subsequently, the electric field intensity $E = -\nabla V$ for any position in the model can be determined. Knowing the electric

field intensity, the energy stored in the electric field between the capacitor plates can be calculated by solving the following integral in COMSOL Multiphysics

$$W_{stored} = \int D.EdV \tag{34}$$

Where W_{stored} $[J]$ is the stored electric energy between the capacitor electrodes. Knowing the stored electric energy, the sensor capacitance can be computed as follows

$$W_{stored} = \frac{1}{2}CV^2 \rightarrow C = \frac{2W_{stored}}{V^2} \tag{35}$$

Where C [F] is the sensor capacitance, and V [V] is the potential distribution across the capacitor terminals.

3.4. Model implementation

3.4.1. Introduction

In this section, a COMSOL Multiphysics model of a capacitive sensor is developed in order to find the optimum sensor configuration. The design process for the capacitive sensor model consists of the following steps:

1. Definition of the model geometry
2. Assignment of model materials and their properties
3. Definition of the boundary conditions
4. Generating a proper mesh
5. Determining the field distribution
6. Using the post processing capabilities of COMSOL Multiphysics to compute the capacitance of the sensor

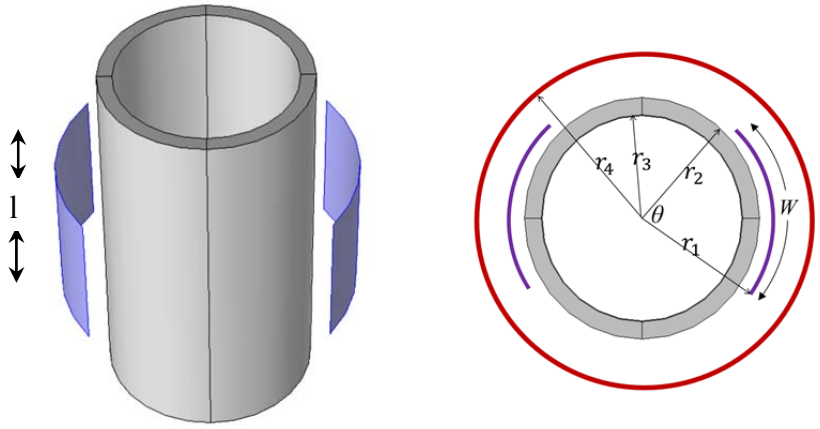

(a) (b)

Figure 3.1: (a) capacitive sensor model schematic diagram where, for simplicity, the earthed screen is not illustrated (b) Cross sectional view of the sensor model. Red circle represents the outer screen.

3.4.2. Geometry

Figure 3.1 shows the configuration of the capacitive sensor model, which consists of two identical curved electrode plates mounted to the exterior of a cylindrical pipe wall. The electrodes have the same curvature as the cylindrical pipe, and the pipe is filled with a dielectric material. An earthed outer screen surrounds the cylindrical pipe in order to protect the capacitive sensor from external electrical interference. The space between the electrodes and the screen can be filled with an insulating material, although in many cases this space is occupied by air [70].

The capacitance between the two electrodes is dependent on both the dielectric properties of the material inside the pipe and geometric properties of the capacitive sensor. The geometric properties include the thickness and diametr of the cylindrical pipe wall and dimension of the curved electrodes. The electrode configuration offers a non-destructive and non-intrusive way of electrostatic field generation across the electrodes, compared to the commonly used intrusive capacitive sensors using electrode plates mounted on the inside of the pipe wall. These internal electrodes increase the sensitivity of the capacitive sensor since they are exposed directly to the dielectric material. They do, however, suffer disadvantages like contamination caused by the flowing medium and erosion. In Figure

3.1 the general capacitance sensor model in which the cylindrical pipe and the electrode can take various radii, is considered.

Table 3.1: Geometric parameters of the sensor model

Parameter	Expression
Pipe radius	r_3
Pipe height	h
Pipe wall thickness	$r_2 - r_3$
Electrode radius	r_1
Electrode length	l
Electrode width	w
Electrode arc angle	θ
Screen radius	r_4

Table 3.1 represents the geometric parameters of the capacitive sensor model. During the simulation, these are the parameters whose values are varied in order to optimize the capacitive sensor model.

3.4.3. Material

The material distributions applied to the simulated model are chosen to be the same as the material distributions in the experimental setup in order to enable verification. The electrical properties of different dielectric materials which are used to fill the cylindrical pipe are given in Table 3.2.

Table 3.2: Relative permittivity ($\boldsymbol{\varepsilon_s}$) and electrical conductivity (σ) of different dielectric materials at 20 °C.

Material	ε_s	σ [S/m]	Reference
Air	1	0	[71]
Distilled water	80	0	[71]
Ethanol/Water x_e[2] $= 0.22$	55.2	0	[72]
Ethanol/Water $x_e = 0.36$	45.2	0	[72]
Ethanol/Water $x_e = 0.54$	36.2	0	[72]
Ethanol/Water $x_e = 0.76$	29.8	0	[72]

3.4.4. Meshing

When performing a simulation in COMSOL Multiphysics, the mesh settings determine the resolution of the finite element mesh used to discretize the model. The finite element method divides the model into small elements of geometrically simple shapes. Since the capacitive sensor model is a 3D model, a free tetrahedral shape is chosen. A finer mesh size than the suggested default setting is defined in order to have a more accurate result. To ensure the accuracy of the mesh, a convergence analysis is conducted such that the model gets solved iteratively on progressively finer meshes until it is seen that the variation in the solution becomes insignificant. Finally, a refined mesh is selected with maximum and minimum tetrahedral sizes of 1 mm and 0.05 mm, respectively. This leads to a model with an appropriately distributed mesh which consists of about 6×10^6 tetrahedral elements. A 2D plot of the COMSOL-generated mesh is shown Figure 3.2.

[2] x_e is the applied mole fraction of ethanol in the ethanol/water mixture.

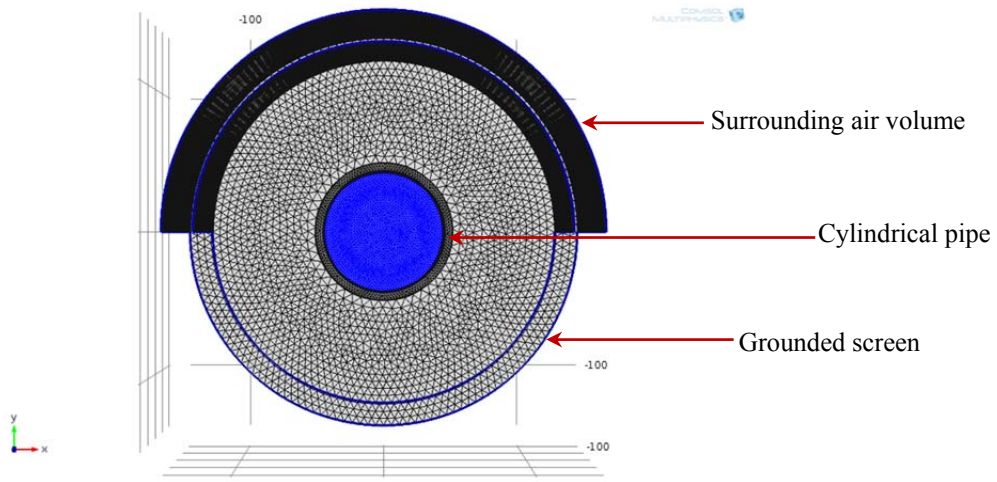

Figure 3.2: 2D tetrahedral mesh plot of the capacitive sensor model. The region of surrounding air and the grounded screen together with the cylindrical pipe is shown in this figure. To get a better view, some of the boundaries are hidden.

3.4.5. Electrical field distribution

The simulation result for the potential distribution and electric field when one electrode is excited (with the excitation frequency of $\omega = 20\,kHz$) and the other electrode together with the outer screen is kept at ground potential is shown in Figure 3.3. The color gradient represents the electric potential distribution at various regions inside the capacitive sensor while the arrows represent the orientation of the electric field. As expected, there is no electric potential outside the grounded screen.

3.4.6. Post-processing

The COMSOL Multiphysics post-processing feature enables the sensor capacitance to be calculated. As discussed in section 3.3, the capacitance can be computed from the stored electric energy which is given by equation (35).

In the following section the post-processing feature is used to calculate the sensor capacitance as a function of various sensor parameters in order to optimize the capacitive sensor model.

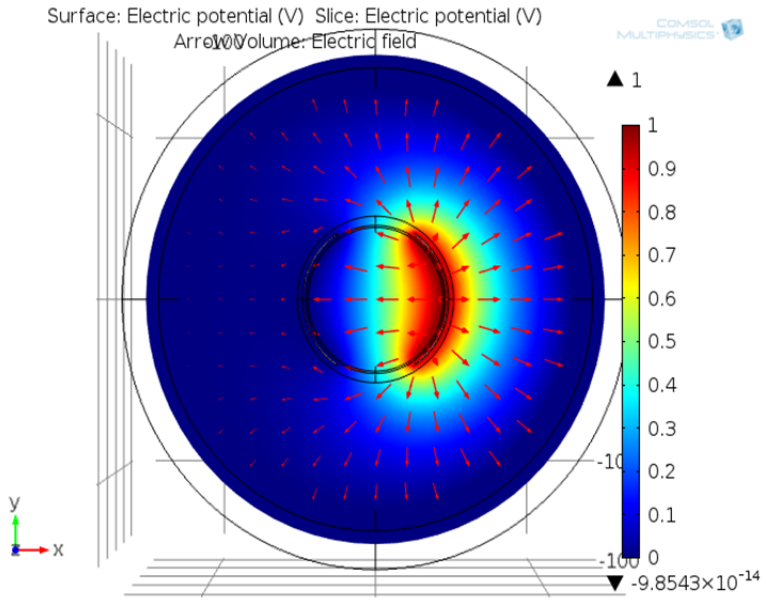

Figure 3.3: 2D potential and electric field distribution of the capacitive sensor.

3.5. Optimization of the sensor model

Optimization of the sensor model is performed by investigating the dependence of the output capacitance on sensor configuration. In order to do this, the effect of electrode configuration and pipe geometry on the sensor output capacitance are investigated in the following sections.

3.5.1. Electrode configuration

This section investigates the dependence of sensor capacitance on the electrode configuration by means of COMSOL Multiphysics solver. The investigated parameters include the electrode length l and the arc angle θ.

The geometric parameters of the cylindrical pipe in the COMSOL Multiphysics model are shown in Table 3.3. The radius, height, and thickness of the cylindrical pipe are chosen for practical reasons. It is assumed that the electrodes are placed on the external wall of the cylindrical pipe i.e. $r_1 = r_2$. By varying the electrode length l and the arc angle θ (see

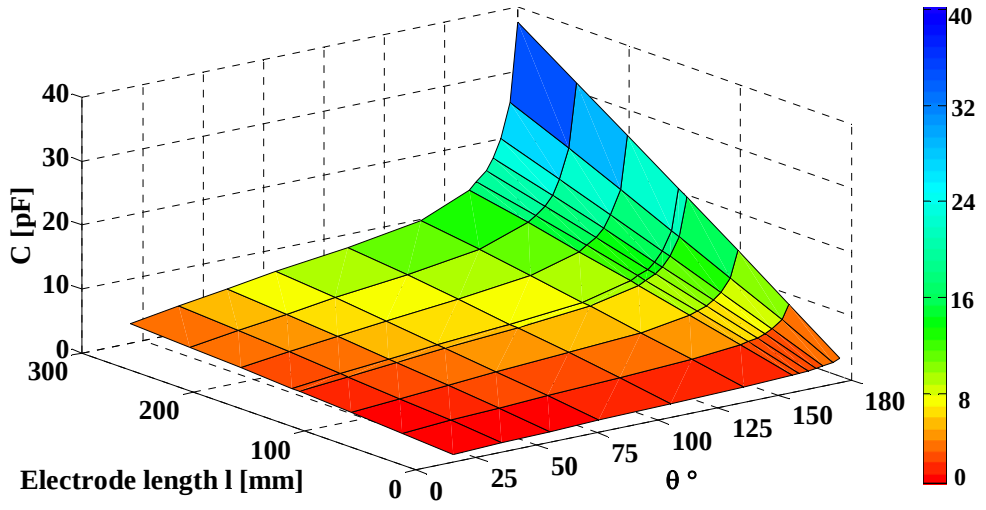

Figure 3.4: Simulated capacitance C as a function of electrode length l and arc angle θ.

Figure 3.1) the capacitance C can be plotted as a function of the electrode configuration (Figure 3.4).

Table 3.3: Specification of the cylindrical pipe.

Radius r_3 $[mm]$	40
Height h $[mm]$	325
Thickness $r_2 - r_3 [mm]$	5
Building material	Plexiglass ($\varepsilon = 2.7$)
Filling material	Empty ($\varepsilon = 1$)

Figure 3.4 shows a positive linear relationship between the capacitance C and the electrode length l for a constant electrode arc angle θ, whereas for a constant electrode length l, the capacitance C increases very quickly and approaches infinity as the electrode arc angle θ tends to 180°.

The reason for this trend is that the charge density on the electrodes increases towards the edges and becomes infinite at the edges of the two electrodes [73]. When the arc angle θ gets close to 180°, the edges of the electrodes are moved closer together. Accordingly, the

gap between the two electrodes becomes very small, and thus the capacitance C tends to increase towards infinity. From Figure 3.4 it can be concluded that the maximum output capacitance can be achieved when the arc angle θ and the length l of the electrodes are as large as practically possible.

As mentioned before, one of the design criteria for the capacitance sensor is to have a sensitive sensor for detecting small permittivity changes of gas hydrate formation over the bulk of the flow under test. In addition, it is known that the gas hydrate formation is not always a homogeneous process, and it takes place in a form of hydrate clusters distributed over the flow. The simulation on the electrode length reveals that the longer the electrode length, the more sensitive the sensor to small changes in the permittivity of the bulk is. However, using too long electrodes can have a disadvantage of yielding the averaged capacitance measurements, and the sensor will not be able to detect all changes due to the hydrate formation. Therefore, we need to make a compromise on the electrode length to ensure an appropriate sensor configuration.

Peng *et al*. [74] investigated the impact of the electrodes' length on the sensitivity distribution in an electric capacitance tomography (ECT) sensor. The sensitivity distribution is one of the key elements for image reconstruction in the ECT sensor, which establishes the relationship between the capacitance measurements and the permittivity distribution. They showed that the sensitivity becomes higher while the length of the electrodes increases. They also showed that if the electrodes are too short (shorter than the characteristic size of the ECT sensor), the sensitivity will be too low. In this paper, it was suggested that the optimal length of the electrodes is when l is the same as the characteristic size of the ECT sensor, which is the diameter of the inner pipe wall for a cylindrical sensor. Since the optimization criterion in this paper was the sensitivity of the sensor in detecting the permittivity distribution, their suggestion on the electrode length can be a good compromise for our sensor configuration. Therefore, the electrode length l can be set to 80 mm, which is equal to the inner cylindrical pipe diameter (see Table 3.3).

As mentioned earlier**,** the capacitance C increases dramatically as θ increases towards 180°. This means that larger values of θ will lead to higher sensitivity. However, when θ

becomes very large, the gap between the electrodes begins to lessen, and consequently the electrostatic field penetration into the dielectric material inside the pipe decreases. To avoid the field penetration issue on one hand, and to achieve a high sensitivity on the other hand, $\theta = 165°$ can be selected as the capacitive sensor arc angle. The reason for this is that $\theta = 165°$ is the angle at which the capacitance starts to increase more rapidly (see Figure 3.4).

3.5.2. Pipe geometry

In this section the dependence of the sensor output capacitance on the pipe geometry is investigated by means of the COMSOL Multiphysics solver. The investigated parameters include the pipe thickness and its diameter.

In order to perform the simulation, the geometric parameters of the electrodes need to be specified. According to Table 3.4 the resultant values discussed in section 3.5.1 are selected as the values of the electrodes' length and arc angle. It is assumed that during the simulation, both electrodes have a constant radius of r_1, and it is also assumed that the pipe is $(\varepsilon = 1)$.

Table 3.4: Specification of the arc electrodes.

Radius r_1 $[mm]$	45
Arc angle θ	165°
Length l $[mm]$	80
Width $\frac{2\pi.\theta}{180} \times r_1$ $[mm]$	130

By varying the pipe diameter and its thickness, the sensor output capacitance can be plotted as a function of the pipe geometry. The diameter and thickness variations are represented by the difference $r_1 - r_2$ (while r_1 remains constant), and the difference $r_2 - r_3$, respectively (see Figure 3.5).

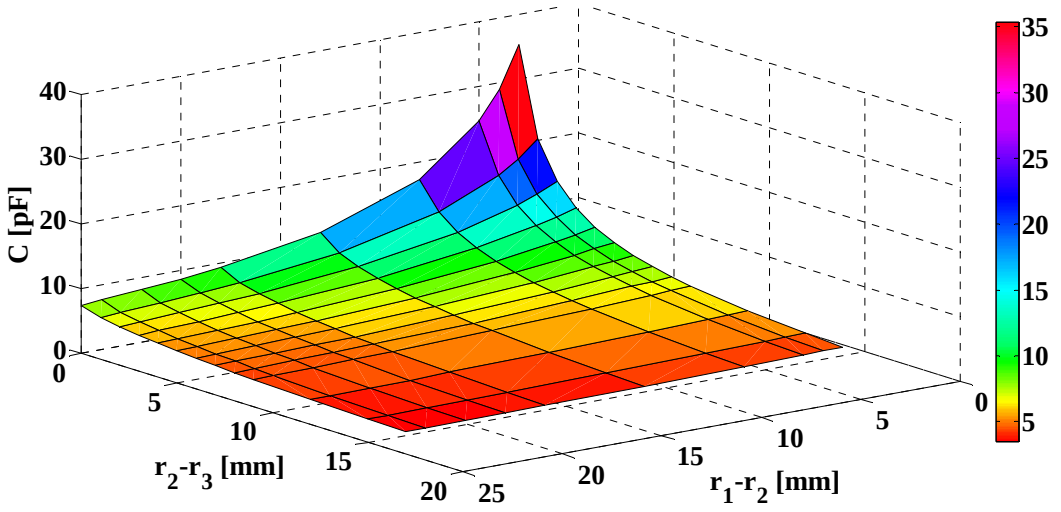

Figure 3.5: Simulated capacitance C as a function of the pipe thickness ($r_2 - r_3$) and diameter ($r_1 - r_2$) (while r_1 remains constant).

It is seen from Figure 3.5 that for a constant thickness, i.e. constant difference $r_2 - r_3$, the sensor output capacitance increases as the difference $r_1 - r_2$ (the gap between the electrodes and external wall of the pipe) decreases, especially when this difference goes toward zero. Figure 3.5 implies that during measurements with a capacitive sensor whose electrodes have the same radius as the pipe, the presence of small air gaps between the electrodes and the external wall of the pipe will contribute a systematic error in the measured capacitance *C*. Therefore, in order to minimize the systematic error due to air gaps between the electrodes and the pipe wall, the electrodes must be in tight surface contact with the pipe wall [75].

Moreover, it is observed from Figure 3.5 that decreasing the difference $r_2 - r_3$ leads to an increase in the sensor capacitance for any constant $r_1 - r_2$. When the difference $r_1 - r_2$ tends to zero, the sensor capacitance grows faster as the difference $r_2 - r_3$ decreases. The reason for this trend is that the computed sensor capacitance of each electrode is actually the series capacitance of the pipe wall capacitances C_w and the internal capacitance C_x which is solely related to the dielectric material inside the pipe [76]. When the difference $r_2 - r_3$ or, in other words, the pipe wall thickness decreases, the influence of

C_w on the computed sensor capacitance is mitigated, and the distance between the sensor electrodes and the dielectric material inside the pipe decreases as well. When $r_1 - r_2 = 0$, the computed sensor capacitance tends to infinity as $r_2 - r_3$ approaches zero, since there is no longer a gap between the electrodes and the dielectric material inside the pipe. In practice, the pipe wall thickness $r_2 - r_3$ is always fixed. Therefore, it is essential to keep the difference $r_1 - r_2$ close to zero to achieve a high sensitivity.

3.5.3. Critical height

It is apparent that for a vertical capacitance sensor, such as the one utilized in this thesis, the dielectric material level should be at least equal to the height of the electrodes. However, to suppress the edge effect[3] on the upper/lower ends of the electrodes, an additional amount of the dielectric material is added to increase the dielectric level up to a critical value. The critical value of dielectric level is where the capacitance becomes independent of the dielectric level variation.

The critical value can be calculated via COMSOL simulations. For this purpose, the electrodes of length l=80 mm are assumed to be located at 40 mm above the bottom of the cylindrical pipe. It is also assumed that the capacitance sensor is filled by water as a dielectric material up to 120 mm (the same as the height of the electrodes' upper edge). The capacitance variation of the sensor is then computed and plotted as the dielectric level increases. As the dielectric level passes a critical value, the capacitance curve gets saturated at a fixed value. As Figure 3.6 shows, this critical value is equal to 170 mm. This implies that the dielectric level should be at least 50 mm beyond the electrodes' edges at either end of the sensor. This conclusion will be taken into account to the experimental setup configuration used in Chapter 4.

[3] Deformation of the electric field lines which is a function of the dielectric permittivity and by the effect of the edges of the electrodes. The edge effect causes the electric field to increase in the edges of the electrodes.

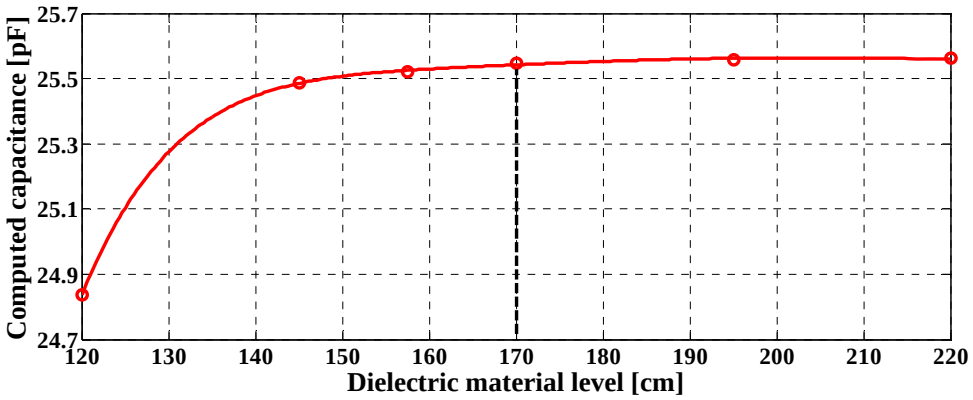

Figure 3.6: Computed capacitance as a function of dielectric material level of height in the capacitance sensor model.

3.5.4. Guard electrodes issues

One of the problems associated with capacitance measurements is the so-called fringing of the electric field (edge effect of the electrodes) [26].The fringing effect occurs when the electric field lines tend to spread out near the edge of the electrodes, which results in a non-uniform electric field at the edges. If the fringe effect does not occur i.e. the capacitor is an ideal sensor, the capacitance value can be readily calculated by Equation (2), assuming a simple parallel plate capacitor. By applying the guard electrodes on non-ideal capacitors, the electric field distribution between the two electrodes remain uniform, and thus, the Equation (2) is applicable to calculate the capacitance value.

The structure of a parallel plate capacitor with guard electrodes is shown in Figure 3.7. As is shown in this figure, if the guard electrodes are kept at the same potential as the sensing electrode but electrically insulated from it, the influence of the fringe field will be eliminated.

In this thesis, it is not intended to use a theoretical equation when measuring the capacitance. Instead, a calibration procedure will be performed (see Section 4.2.1). Therefore, it is not needed to use the guard electrodes to deal with the fringing effect.

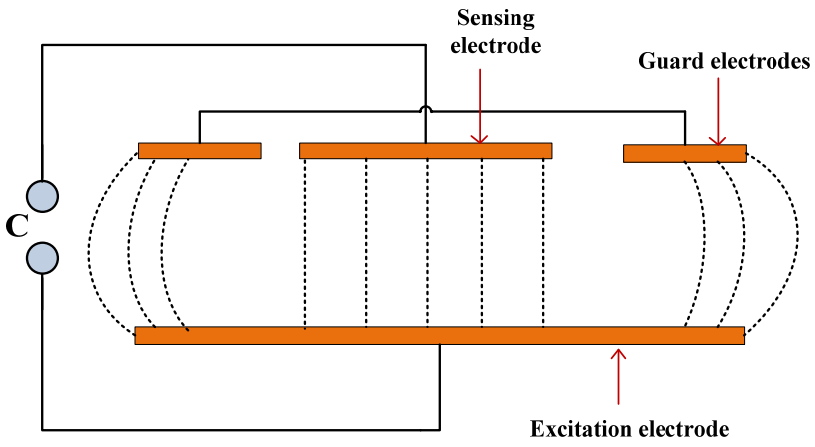

Figure 3.7: Parallel plate capacitance sensor with guard electrodes.

3.6. Construction of the capacitive sensor

So far, modeling a curved-electrode capacitance sensor was explained. The aim of modeling was to find an appropriate sensor configuration design, in order to construct an experimental capacitance sensor setup (Figure 3.8). This experimental setup will then be utilized for permittivity measurements of gas hydrates.

3.6.1. Fundamental elements

Fabrication of the capacitive sensor was carried out at the mechanical workshop, the Department of Physics and Technology, University of Bergen. The capacitive sensor setup comprises two identical conducting curved electrodes mounted on the outside of a non-conductive pipe, surrounded by an electrical screen. The electrodes were made of a flexible and self-adhesive copper tape (3M™ 1126 Tape) with a width and thickness of 76.2 mm and 0.088mm, respectively, which could be cut to any desired length to conform to the simulated results. A photograph of the experimental setup is shown in Figure 3.8. The sensor setup design characteristics are listed in Table 3.5.

Table 3.5: Characteristics of the sensor setup design.

Length of electrodes:	80 mm
Electrode angle:	165°
Width of electrodes:	130 mm
Distance from bottom of pipe to electrode lower edge	50 mm
Distance from centre of pipe to screen:	120mm
Distance from centre of pipe to pipe wall:	45 mm
Distance from the pipe wall to screen:	75 mm
Pipe wall thickness:	5 mm
Dielectric constant of pipe wall (Plexiglass):	2.7
Screen thickness:	1 mm
Guard electrodes used:	None

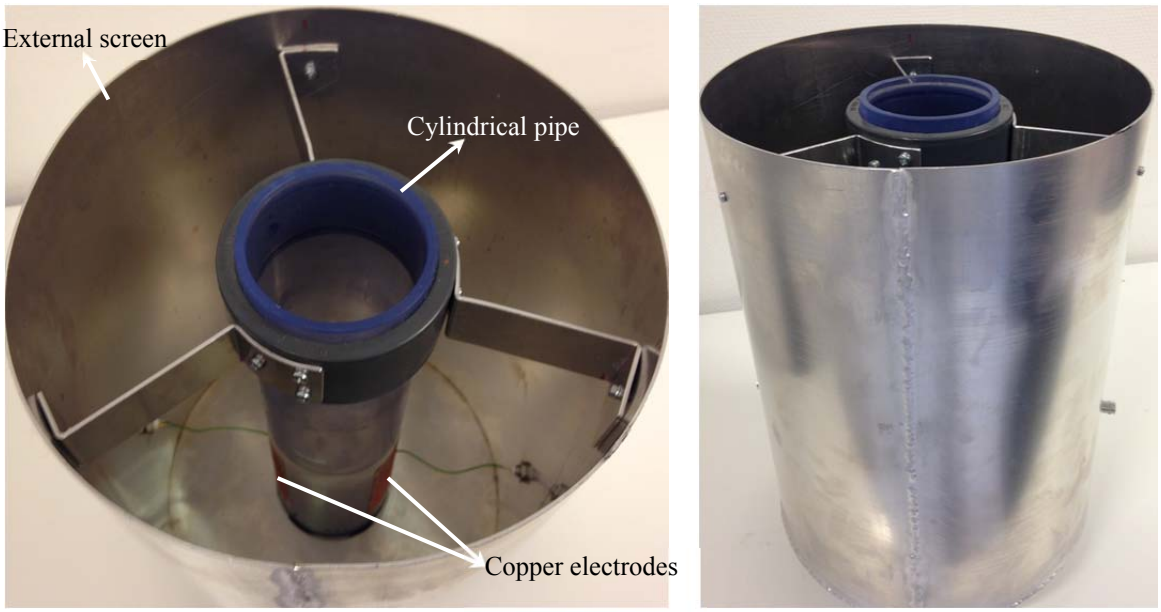

Figure 3.8: Photograph of the experimental setup.

According to the electrodes' specification (Table 3.5), a pair of 80×130 cm copper tape strips were cut and glued onto the outer surface of a cylindrical pipe (see Figure 3.8). The copper electrodes were aligned carefully so that:

- the upper and lower edges of the two electrodes were at the same height
- the vertical edges of both electrodes were parallel with each other
- the two vertical gaps between the two electrodes were of the same size.

As concluded in Section 3.5.2, the air gaps between the electrodes and the pipe wall can cause a systematic error in the capacitance measurement. For this reason, in gluing the copper strips to the pipe walls air gaps were minimized.

The cylindrical pipe was made of plexiglass and a drainage valve was mounted at the bottom to allow easy emptying of the pipe.

An aluminum cylinder box surrounding the pipe was added as an external screen in order to minimize the effects of external electrical interference and standing capacitance. The screen radius was selected to be three times the radius of the electrodes. The reason for such a selection is that if the screen radius is not sufficiently large compared to the sensor radius, the stray capacitance introduced between the electrodes and the earthed screen can be coupled with the capacitive effect through the sensing region of the capacitance sensor.

3.6.2. Connections

As will be explained in the next chapter, an impedance measurement instrument (impedance analyzer) is used for measuring the capacitance C between the electrode plates. To measure the capacitance by means of the impedance instrument, a voltage difference needs to be applied across the electrodes such that one electrode (sensing electrode) is grounded and the other electrode (excitation electrode) is kept at a non-zero voltage. Moreover, the external screen must be grounded to act as an electrical shield.

In order to connect the impedance analyzer to the capacitive sensor, two BNC plugs are mounted on opposite sides of the external screen wall.

One of the BNC plugs (isolated) is connected to the excitation electrode through its centre contact by a soldered copper wire on one side, and to the high voltage terminal of the impedance analyzer by a coaxial cable on the other side.

The other BNC plug (with no insulation in the centre) is connected to the sensing electrode by a soldered copper wire on one side, and to the low voltage terminal (ground) of the impedance analyzer by coaxial cable on the other side. Since a BNC plug without insulation is used, the external screen is also connected to the low voltage terminal (ground).

3.7. Verification of the simulation model

To determine if the sensor model can be an acceptable representation of a real sensor, the validity of the sensor model should be first verified. To verify the model, the simulated results should be compared with the experimental values obtained from the experimental setup. If the simulation results are in a reasonable agreement with the experimental data, it implies that the obtained configurations can be reliable and valid in practice. To do so, an experimental capacitance sensor setup is constructed to match a sensor configuration used in a sensor simulation (the construction of capacitance sensor setup was explained in Section 3.6). Then, the capacitances of a number of dielectric materials of known permittivity are determined using both the sensor model in the COMSOL Multiphysics environment and the experimental setup. The results are plotted in Figure 3.9. In this Figure, the experimental and simulated results are shown as the difference between the capacitance of the reference samples (C) and the capacitance of the empty sensor (C_{air}). The difference between the simulated and experimental capacitance of the empty sensor are $(C_{simulation} - C_{experiment})_{air} = 4.5\ pF$.

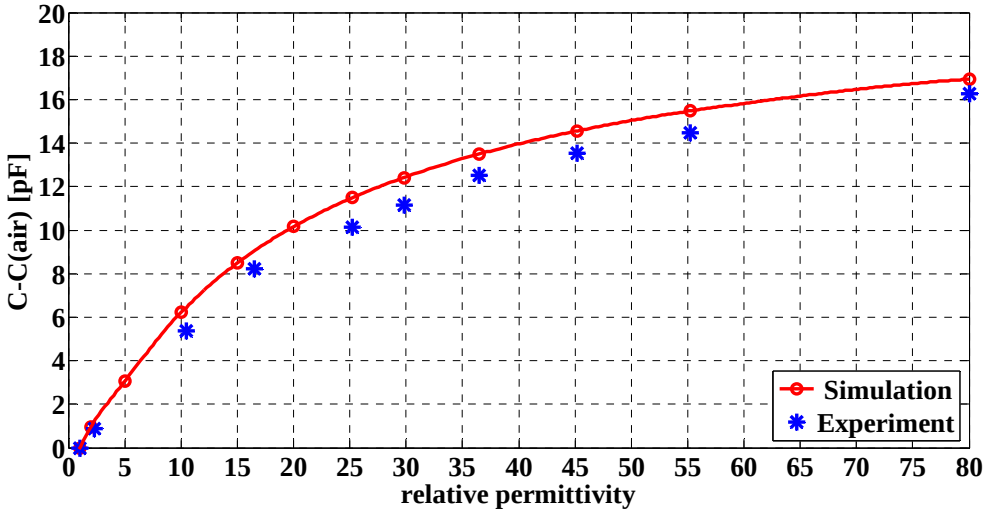

Figure 3.9: Measured and simulated differential capacitance of reference samples as a function of permittivity. The vertical axis shows the difference between the capacitance of reference samples and the empty sensor capacitance for both the experimental and simulated results.

Comparing the simulated and experimental capacitance in Figure 3.9 shows a good trend with an offset which can be due to existence of parasitic capacitances that appear in some circuit parts and influence or alter the true capacitance measurement. There are different sources of parasitic capacitances in series or in parallel with the measured capacitance which are inevitable, even though the capacitance measuring instrument is stray-immune. These sources can be parasitic capacitance between the capacitance sensor electrodes and the grounded external screen, parasitic capacitance of the coaxial cables that transport the electrical signals or parasitic capacitance of the CMOS keys [77]. By assuming that the deviation of the experimental from simulation results can be attributed to the existence of parasitic sources, it can be concluded that the simulation and the experiment are in a good agreement. Therefore, the experimental setup constructed based on the configuration derived from simulation can be reliable for performing further measurements in the following chapters.

4. Experimental Setup and Procedure

This chapter mainly focuses on two parts: First, the overall hydrate forming experimental process will be explained. Second, the apparatus and experimental procedures of permittivity measurements during hydrate formation will be described thoroughly.

4.1. Preparation of hydrate forming emulsions

In order to perform permittivity measurements in water/oil emulsions with gas hydrates, hydrate forming emulsions need to be made first. To make the emulsions, Cyclopentane (C_5H_{10}) was chosen as an appropriate hydrate former serving as the oil phase of the emulsions. The reason for choosing Cyclopentane (here-after CP) is that it forms structure II hydrates at atmospheric pressure with hydrate formation equilibrium temperature of about 7 °C [78, 79]. Therefore, working with high pressure equipment and flammable gases is avoided. Because CP forms the structure-II hydrates [80] usually encountered in petroleum fields, CP hydrates serve as a good atmospheric model in hydrate related studies [79, 81-83].

In this thesis, the intention was to study two water-oil emulsions with different phase fractions: (1) an emulsion with β=70% water fraction and (2) an emulsion with β=40% water fraction prepared by adding Span80 (1.0% volume of the mixture) as the emulsifier for stabilization of the mixture. It should be noted here that as explained in Section 2.2.4, the capacitance sensor setup will not work for water continuous emulsions due to the short circuiting effect of sensor electrodes in the presence of any conductivity in the water phase. Therefore, distilled water was used for making the emulsions. Table 4.1 lists the specification of the hydrate forming emulsions used in this thesis.

Table 4.1: Specification of hydrate forming cyclopentane/water emulsions.

Sample no.	Composition (% on volume basis)		
	Cyclopentane	Water	Span80
i	30	70	-
ii	59.5	39.5	1

On the basis of the sensor design outlined in Section 3.5.3, 800 ml of emulsion was required to fill the cylindrical vessel above the upper edge of electrodes. By adding the corresponding proportion of distilled water and CP (for instance in the case of 70% water-in-oil emulsion: 560 ml distilled water and 240 ml CP), and continuously stirring the resulting mixture, a homogeneous emulsion was obtained. For making the oil continuous emulsion, it was necessary to mix Span80 with CP first, and then add distilled water to the mixture in order to obtain a homogeneous emulsion. Formation of CP hydrate can take place if the emulsion is kept at a suitably sub-cooled temperature. Since the equilibrium temperature for CP hydrate formation is about 7 °C at atmospheric pressure [78], the emulsion should be cooled down below this temperature. On the other hand, the temperature of the emulsion should be kept at positive temperatures, because existence of the liquid phase of water in the emulsion is a basic requirement for CP hydrate formation. Accordingly, the temperature of the emulsions was maintained at 3 °C at the beginning of the experiments. Because it is difficult to initiate CP hydrate formation without adding a promoter (such as ice, rust, chalk, clay etc.) [84] within a time frame of 24 hours, a small piece of distilled water ice was made and kept in freezer to be added to the emulsion later on to trigger CP hydrate formation.

Having described the preparation of CP hydrate emulsions, the next section will describe the apparatus and experimental procedures employed for permittivity measurements during CP hydrate formation.

4.2. Instrumentation and data acquisition

The experimental work was carried out in the chemistry laboratory at Christian Michelsen Research (CMR). The experimental apparatus used for monitoring permittivity changes during CP hydrate formation is shown in Figure 4.1. The main equipment employed in the experiments consists of:

- A curved electrode capacitance sensor (Chapter 3)
- Two thermocouples (Type-K NiAl/NiCr)
- Temperature chamber (WTB Binder)
- Magnetic stirrer (Franz Morat R16)
- Impedance analyzer (Agilent HP 4192A LF)
- Laptop (Dell Latitude E5500)

To monitor the formation of CP hydrates, the variations of two parameters, capacitance C and temperature T, of the hydrate forming emulsions need to be monitored.

To do so, the cylindrical vessel of the capacitance sensor was filled with the hydrate forming emulsion in order to perform capacitance measurements.

An impedance analyzer was employed to measure the capacitance between the two electrodes of the capacitance sensor. The measured data were transferred into an external PC via an Ethernet (LAN) interface for further analysis including data post-processing using MATLAB. The impedance analyzer operating frequency was set at 20, 120, 220, 320, 420, 520, 620 and 720 kHz to cover the kHz frequency range. A Python software code was used for data acquisition between the impedance analyzer and the external PC such that the capacitance C was measured and recorded at the specified frequencies every 15 seconds.

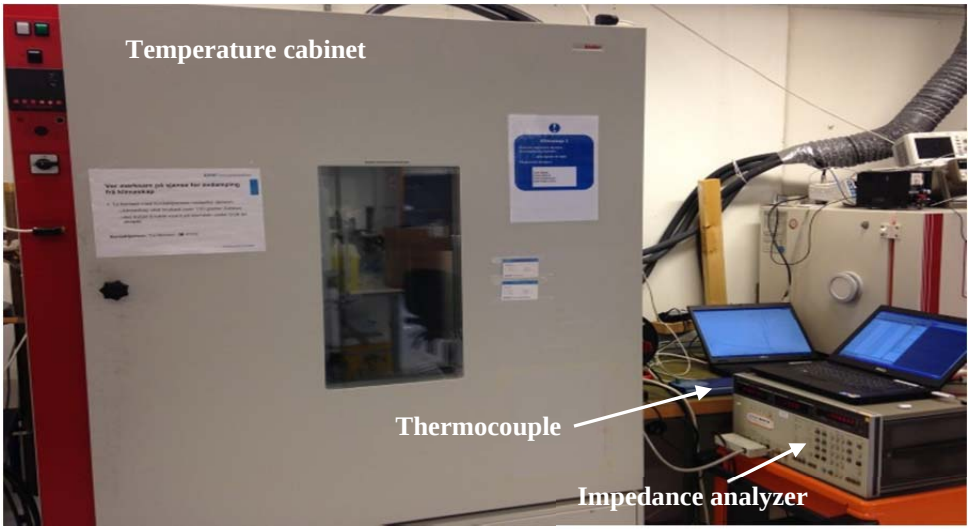

(a)

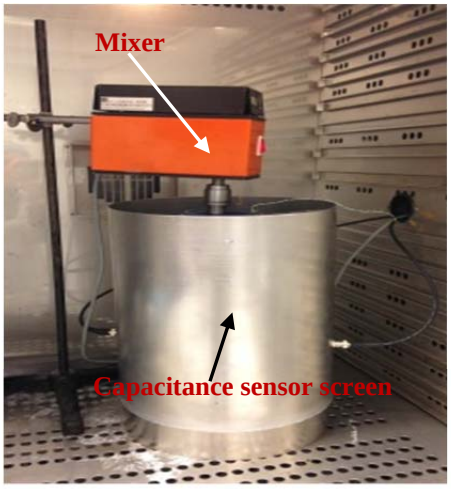

(b)

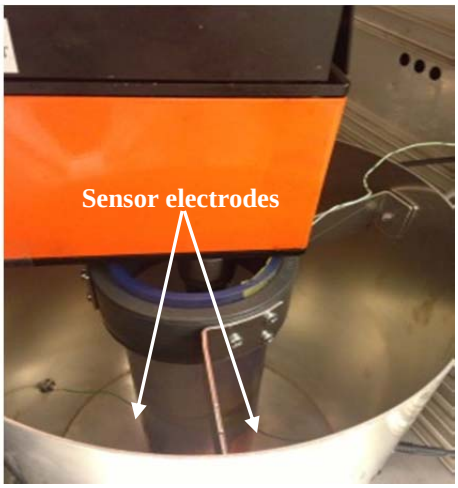

(c)

Figure 4.1: (a) Photograph of the experimental apparatus used for monitoring CP hydrate formation. The capacitance sensor is placed inside the temperature cabinet to control its temperature. The temperature thermocouples and the coaxial connections between the analyzer and the sensor are inserted inside the cabinet via a hole in its wall. (b) Photograph of the capacitance sensor and the mixer inside the temperature cabinet. In this figure, the outer screen of the sensor is only visible. (c) Top view of the capacitance sensor. The connecting wires between the electrodes and the inner wall of the screen can be seen.

The capacitance sensor was placed inside a temperature chamber, which is capable of controlling the temperature over a range of ±30 °C, to expose the emulsion to different temperatures. A mixer was also installed inside the temperature chamber to agitate the contents of the vessel at 120 rpm such that the contents were held in the state of an emulsion. The stainless steel arm of the stirrer had to be replaced with a non-conductive

rod, since the capacitance measurements would be affected by the electric conductivity due to presence of a conductive object between the electrodes of the sensor [85]. Hence, a nylon rod was used, and its blades were made using two nylon cable ties glued to the bottom of it. The space between the blades and the inner wall of the vessel was about 20 mm.

Two thermocouples were inserted into the temperature chamber; one was fixed on the inner wall of the cylindrical vessel of the capacitance sensor for continuously measuring and recording the chronological temperature variation of the emulsion during the CP hydrate formation experiment. To avoid the thermocouple getting stuck to the stirrer, we had to fix the thermocouple end by gluing it to the inner wall of the vessel such that it could provide direct contact with the vessel contents to accurately measure and record the temperature of the emulsion. The other thermocouple was used for recording any temperature variations inside the temperature chamber while opening and closing the chamber door for visual observation.

So far, the requirements for conducting permittivity measurement experiments including preparation of test samples and explanation of the experimental apparatus were explained. The next section describes the experimental procedure used to perform the experiments.

4.2.1. Calibration of the capacitance sensor

As mentioned before, the aim of this thesis is to investigate the formation of gas hydrates by measuring permittivity variations. To do so, permittivity data should be derived from the capacitance values, C, measured by the impedance analyzer. In order to find permittivity data from the measured capacitance, C, a calibration procedure of the capacitance sensor needs to be performed first.

The calibration procedure yields a relationship between the permittivity ε of the sample under test and the capacitance sensor output C namely $C = f(\varepsilon)$. This relationship is reflected in a capacitance-permittivity curve called calibration curve.

To find the calibration curve, a series of capacitance measurements were conducted on different samples of known permittivity (reference samples), Table 4.2, found from literature data. To perform the calibration measurements, certain conditions should be met. For instance, based on the sensor design in Chapter 3, the volume of reference samples prepared for the experiment was 800 ml. Since the calibration measurements were performed at room temperature (T=20° C), the corresponding values for permittivity of reference samples at this specific temperature were considered (Table 4.2). Moreover, since the operating frequency range of the experiments was in the kHz range, the low frequency (static) values of the permittivity ε_s were selected from the literature data. In addition, distilled water (water with no conductivity) was used both for making the emulsions and when the water was the reference sample per se. This is due to the limitation in using capacitance sensors with conductive materials (see Section 2.2.4).

Table 4.2: Permittivity data of reference samples at 20° C found in the literature.

Material	ε_s	$\sigma[S/m]$	Reference
Distilled water	80	0	[71]
Ethanol/Water x_e[4] $= 0.22$	55.2	0	[72]
Ethanol/Water $x_e = 0.36$	45.2	0	[72]
Ethanol/Water $x_e = 0.54$	36.2	0	[72]
Ethanol/Water $x_e = 0.76$	29.8	0	[72]
Ethanol	25.2	0	[71]
Ethanol/Octanol $x_e = 0.5$	16.5	0	[86]
1-Octanol	10.30	0	[13]
Diesel	2.3	0	[13]
Air	1	0	[71]

[4] x_e is the applied mole fraction of ethanol in the mixture

After the desired amount of all reference samples were prepared, capacitance measurements were performed for each sample, and the frequency was swept between 20 kHz to 800 kHz at intervals of 20 kHz. To verify the performance of the sensor, each measurement was repeated 10 times at each frequency. Under the aforementioned conditions, the curves of capacitance-frequency were plotted which is shown in Figure 4.2. This figure plots the average value of the measured capacitance of 10 different reference samples in the frequency range from 20 kHz to 800 kHz. Figure 4.3 shows the standard deviations of 10 measurements of capacitance for all reference samples. The figure shows less than 0.02 in standard deviation in the repeated measurements.

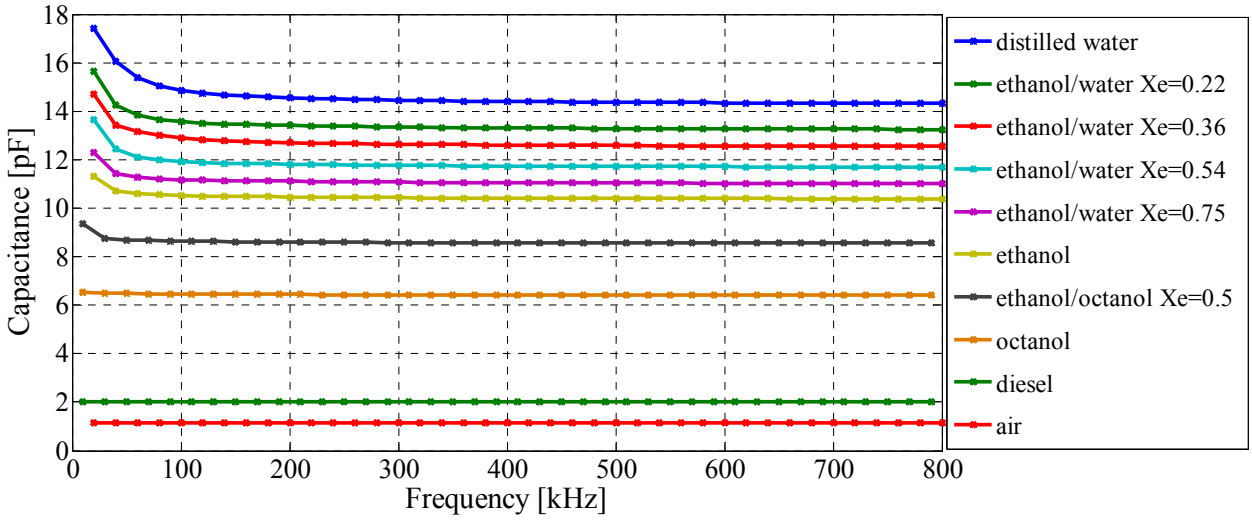

Figure 4.2: Average capacitance in 10 repeated measurements of 10 reference samples as a function of frequency.

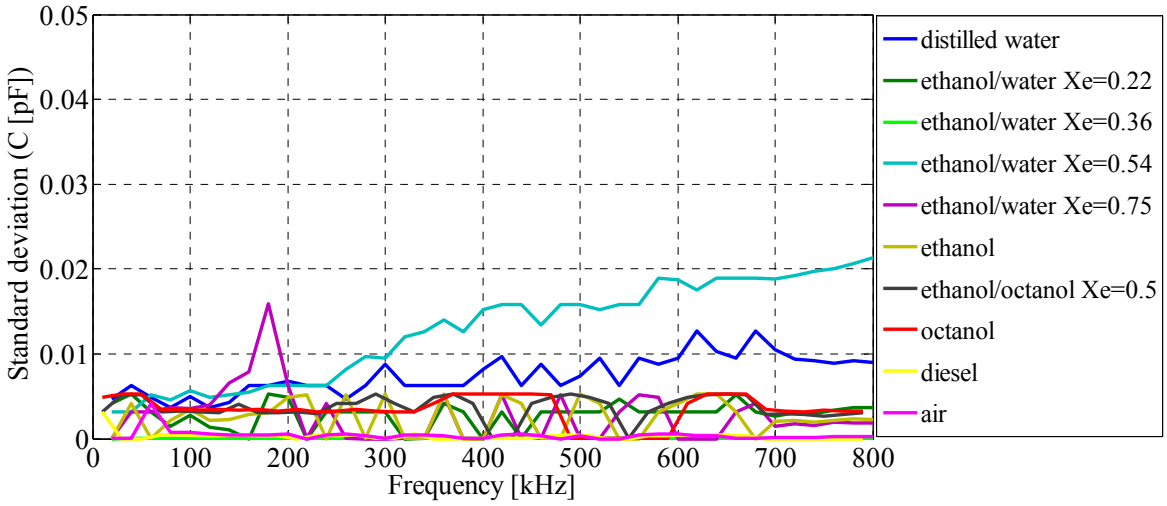

Figure 4.3: Standard deviations in 10 repeated measurements of capacitance for 10 reference samples in the frequency range of kHz.

To obtain the sensor calibration curve $C(\varepsilon)$, the capacitance values of all reference samples were derived at each frequency (from 20 kHz to 800 kHz at intervals of 20 kHz) from Figure 4.2, and the capacitance values were plotted as a function of corresponding permittivity from Table 4.2 (See Figure 4.4).

By using the MATLAB curve fitting tool box, the best fitted curves were generated for each data set along with the equivalent best-fit polynomial equations. In Figure 4.4, the best fitted curve and the equivalent equation are only shown at one frequency. The norm of the residuals was calculated for the polynomial fits to provide a measure of fit quality (Figure 4.5).

Since the best fitted curves are injective (one-to-one), we can calculate the inverse of fitted equations to achieve the permittivity-capacitance relation $\varepsilon = f^{-1}(c)$. Now, it is possible to estimate the permittivity of unknown samples from measured capacitance data.

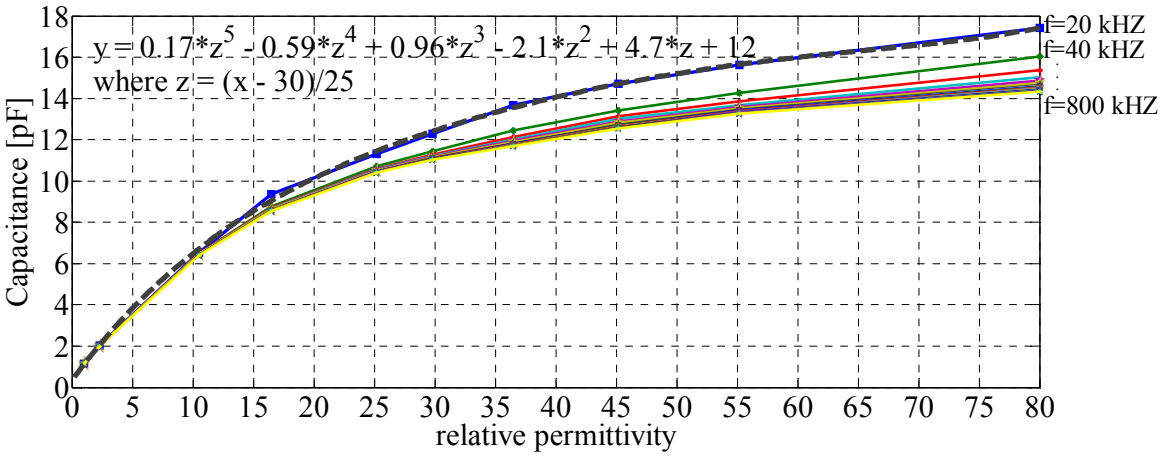

Figure 4.4: The capacitance sensor calibration curves at different frequencies in the kHz region. The black dashed line indicates a fifth-order polynomial curve fitted to the measured capacitance data at f=20 kHz. The corresponding best-fit polynomial equation is written on the top of the curve.

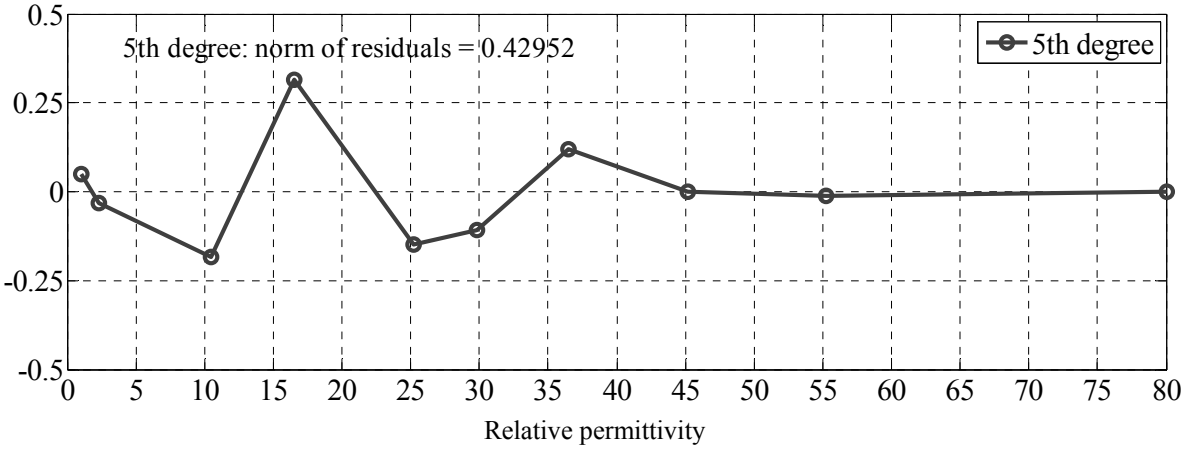

Figure 4.5: The norm of residuals of the fitted curve at f=20 kHz is 0.43 which indicates that the quality of the fit is good. The figure indicates that for large permittivity values, the fifth-order polynomial is best fitted to the measured capacitance data.

4.3. Monitoring permittivity changes during CP hydrate formation

As mentioned in the previous Section, two hydrate forming test samples were prepared in order to investigate permittivity variations during hydrate formation phenomenon. These samples were different with regard to their component fraction; an oil continuous emulsion with 40% water fraction, and a water continuous emulsion with 70% water fraction.

The experimental procedure for permittivity measurements of the water continuous emulsion began with locating the capacitance sensor inside the temperature chamber whose temperature was set at 3 °C. The cylindrical vessel of the capacitance sensor was then filled with the emulsion which had been kept in the refrigerator. The emulsion was continuously agitated by the stirrer to have a homogeneous mixture during the experiment. After the temperature of both chamber and emulsion was stabilized at about 3 °C, the CP hydrate formation was triggered by adding a small piece of ice. After the CP hydrate formation was completed, the emulsion was heated in order to melt the formed CP hydrate. To ensure that CP hydrate melting was complete, the temperature of the emulsion was increased up to 20 °C which was far above the CP hydrate melting point ($T \approx 7.7$ °C). The temperature T and the capacitance C of the emulsion were continuously measured and recorded during the 24-hour experiment. Visual observations were also performed by opening the temperature chamber's door. The experimental procedure for the second test sample (oil continuous emulsion) was identical to that explained for the water continuous emulsion with the following exception: The capacitance sensor was filled with the second emulsion while the emulsion had not been cooled this time. Hence, it took substantially longer time to have both the emulsion and the chamber stabilized at 3 °C.

The experimental results and their analysis are explained in the next chapter.

5. Results and Discussion

In Chapter 4, the experimental procedure for permittivity measurements of hydrate forming emulsions were explained. The results of these experiments are presented and discussed in this chapter.

As explained in Section 1.3 one of the objectives of this thesis is to investigate the permittivity variation of gas hydrate formation for a range of operating conditions. The effect of changes of water fractions in emulsions and operating frequency are of particular interest. To achieve this goal, the permittivity measurements over a frequency range of 20 to 720 kHz were performed on two oil-water test samples of different water fractions:

- 70% water/30%oil, water continuous emulsion
- 40%water/60%oil, oil continuous emulsion

Capacitance sensors cannot be used to meter water continuous flows in most industrial applications. This is because using water continuous samples will short circuit the capacitance sensor and render it useless (See Section 2.2.4). This problem occurs when the water phase in the sample is electrically conductive ($\sigma \neq 0$). Water in most industrial situations e.g. tap water, sea water, etc. has a non-zero electrical conductivity. Therefore, the capacitance sensor is not a practical measurement instrument when measuring a water containing sample. However, in the laboratory, capacitance measurements can be performed on samples containing distilled water whose conductivity is equal to zero. However, the information derived from the capacitance measurements of non-conductive water continuous emulsions will not represent the performance of the sensor when used in an industrial environment.

Nevertheless, in this thesis, using a non-conductive water continuous emulsion has some advantages. Since this is the first experiment of its kind, it is important to choose the test samples that are likely to give measurable results. The more water content in the samples is, the more hydrates are formed, which may result in a larger and more detectable

permittivity change. In addition, using only the oil continuous emulsions requires a high consumption of the oil phase (cyclopentane) which is costly.

The experimental results on monitoring hydrate formation via permittivity measurements of both the water continuous and the oil continuous sample tests are explained in Sections 5.1 and 5.2 respectively.

Prior to analyzing the measured permittivity changes, and correlating them to the hydrate formation phenomenon, it is necessary to ensure that these variations are only due to the temperature dependent reactions happening in the emulsion. To do so, the capacitance of the empty sensor was measured continuously while the temperature of the sensor was cycled between 20 °C and 3 °C. The measured capacitance was found to be constant over the temperature range studied (Figure 5.1). Therefore, it can be concluded that the capacitance/permittivity variations measured by the sensor was only derived from the process of hydrate formation.

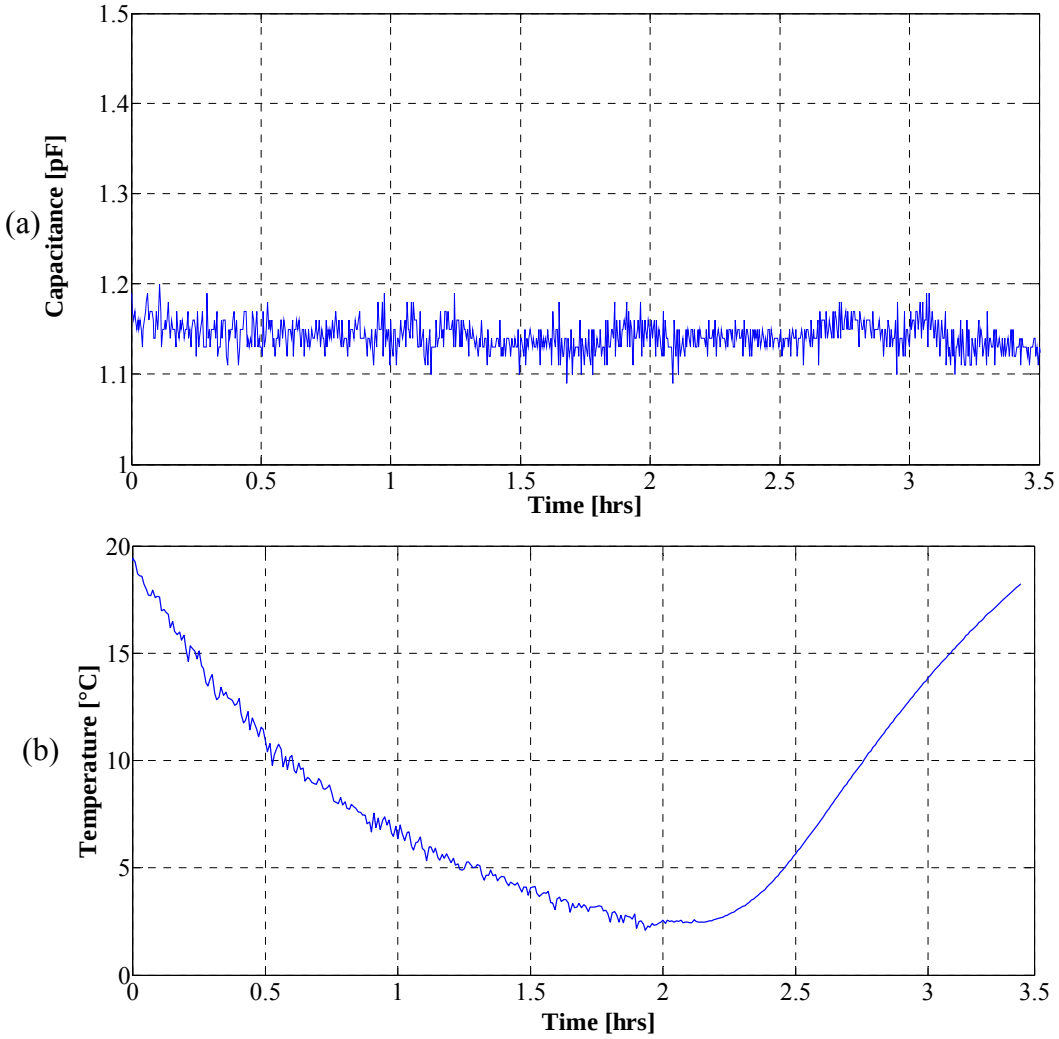

Figure 5.1: Measured capacitance of the empty sensor for varying temperature.

5.1. Permittivity measurements on water continuous emulsion

In Chapter 4, the experimental procedure to be followed in measuring the permittivity changes during hydrate formation in a water continuous sample was explained. During the process of hydrate formation, the data were recorded every 15 seconds over 22 hours for 8 different frequencies between 20 and 720 kHz. The measured capacitance and temperature data are plotted as a function of time. Results are shown in Figure 5.2 (a) and Figure 5.2 (b), respectively. Finally, the corresponding permittivity values calculated from the calibration curve (Section 4.2.1) is plotted in Figure 5.2 (c).

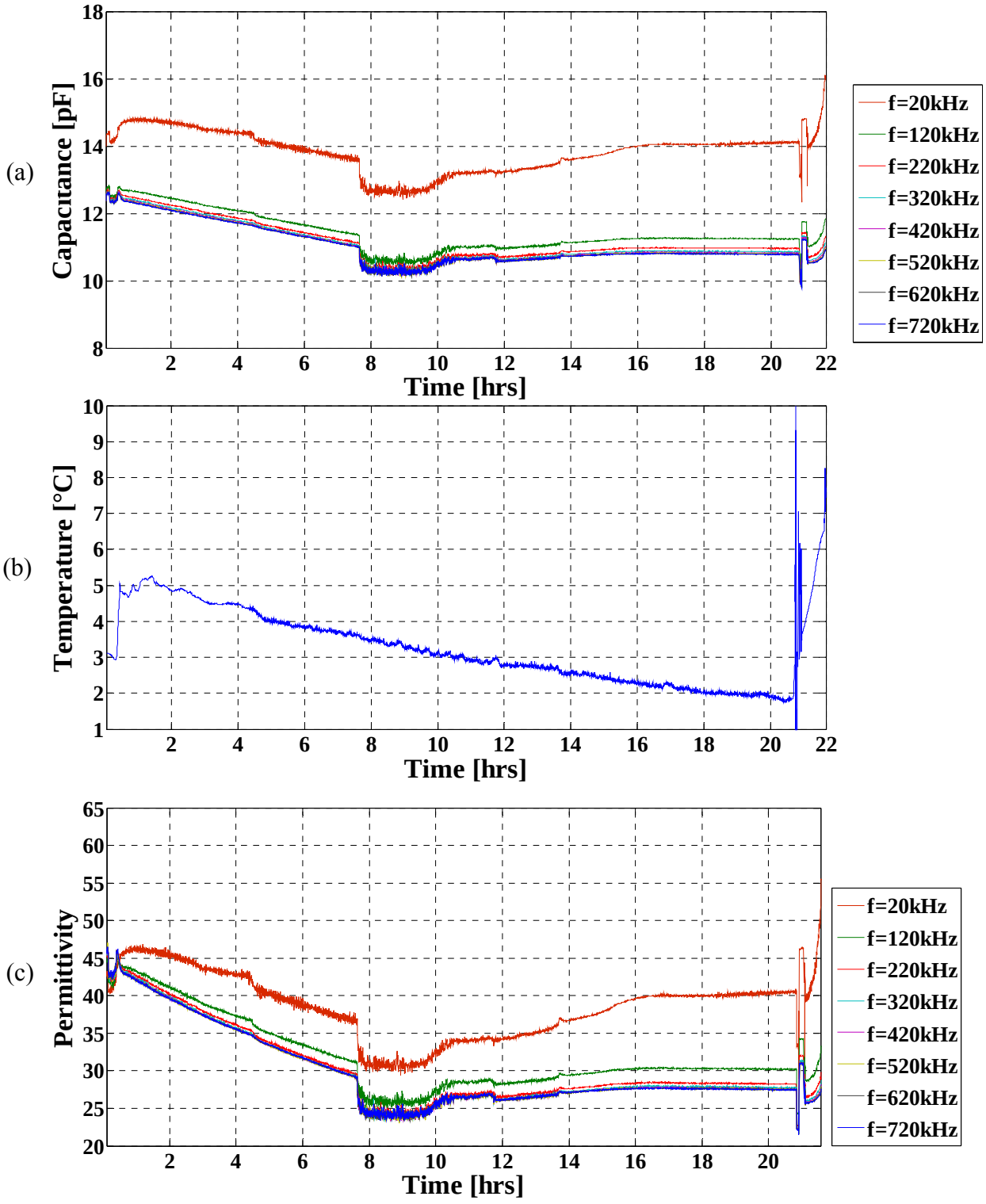

Figure 5.2: (a) Capacitance measurements as a function of time for 10 frequencies between 20 and 720 kHz. (b) Temperature history of test sample. (c) Permittivity data as a function of time.

5.1.1. Analyzing the experimental results

As mentioned in Section 2.1.2, the existence of free water molecules along with hydrocarbons at certain temperatures and pressures will result in the formation of hydrates. Cyclopentane hydrate is reported to form at atmospheric pressure with hydrate formation equilibrium temperature of about 7 °C [78]. To initiate the formation of hydrate, the temperature of the sample needed to be maintained constant at a temperature below the equilibrium temperature. Therefore, the sample was kept at T=3 °C, and a piece of ice was then added to the emulsion to trigger hydrate formation. A couple of minutes after adding the ice, the emulsion underwent an increase in temperature of several degrees (See Figure 5.3 (b)) accompanied by a corresponding sudden increase in the measured permittivity of the emulsion. The temperature rise is a result of the exothermic nature of the physical reactions in the hydrate formation process. Therefore, the temperature rise can be an indication of the onset of hydrate formation. As the permittivity change occurred at exactly the same time at which the temperature increased, it can be said that this change is related to the morphology of the hydrate formation, and can be a determination of the hydrate formation onset.

Before the onset of hydrate formation, a slight increase in the measured permittivity can be seen. This may be due to the fact that Cyclopentane is a volatile substance, and its evaporation at the beginning of the experiment can lead to an increase in permittivity of the emulsion because of the water fraction rise. After the onset of hydrate formation, the measured permittivity shows a gradual decrease at the frequency of 20 kHz, and a sharp decrease at frequencies above 20 kHz. The reason for such a decrease is that with the formation of hydrate, the free water molecules are involved in hydrate formation which results in a reduction in amount of the free water molecules. By decreasing the amount of free water molecules, the overall permittivity of the emulsion reduces correspondingly. The permittivity reduction continues gradually until all water molecules are employed in the formation of hydrate.

However, at t=7.7 h (see Figure 5.2 (c)), a sudden permittivity drop can be seen followed by a plateau lasting for about 2 hours. At this time, the mixer's rod was found to be broken due to turning the liquid emulsion into slurry. It is likely that this accident separated out

the emulsion into the water at the bottom and the hydrate plus the remaining Cyclopentane on the top of the mixture[5]. Therefore, the permittivity measured by the electrodes could be that of the hydrate and Cyclopentane mixture.

After the permittivity plateau, there is a gradual increase in permittivity which is probably due to evaporation of the remaining Cyclopentane in the mixture. At t=16 h the measured permittivity becomes stable, which can indicate that the formation of hydrate has been completed. By completion of the hydrate formation, it is likely that all the water content of the emulsion were converted to hydrate, and the substance remained in the sensor would be a pure hydrate.

At t=21 h, the hydrate was heated up to 15 °C. By increasing the temperature of the Cyclopentane hydrate, it began to melt which resulted in a release of the water molecules involved in the formation of the hydrate structure. As Figure 5.2 (c) shows, the permittivity increase at t>21 h can confirm the melting process of the hydrate. After the melting process of the hydrate is complete, it is expected that the emulsion turns into separate phases of oil and water, and the measured permittivity becomes stabilized. However, the experiment was terminated because the thermocouple became detached from the inner wall of the pipe, and therefore, we have no data related to the complete melting process of the hydrate in the emulsion.

The temperature peak at t=21 h in Figure 5.2 (b) corresponds to the instant that the temperature cabinet was opened in order to compress the emulsion to fill the volume between the two sensor electrodes.

[5] The density of Cyclopentane hydrate is lower than that of water.

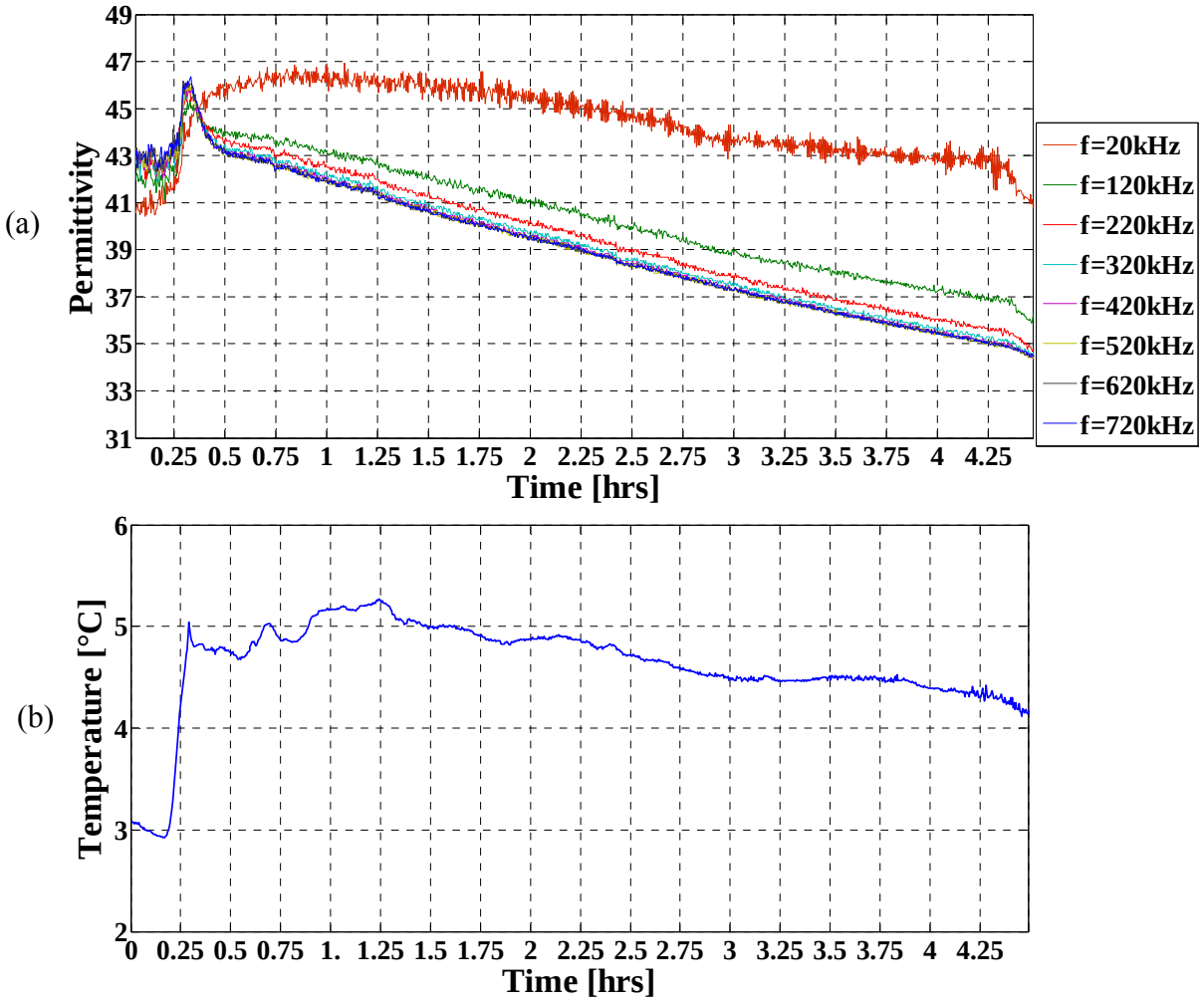

Figure 5.3: (a) Measured permittivity during the first 4.5 hours. (b) Temperature history of the emulsion during the first 4.5 hours.

From Figure 5.2 (c) it is apparent that the permittivity of the emulsion has a frequency dependent behavior. To investigate this dependency, the permittivity spectra at t=4 h (where the hydrate formation is ongoing) and t=18 h (where it is assumed that the hydrate formation is almost complete) are plotted in Figure 5.4.

The permittivity dispersion[6] is only dependent on the volume fraction of free water. Therefore, the change in permittivity is a direct measure of the formation of gas hydrates.

[6] The dependence of the permittivity of a dielectric material on the frequency is called the *permittivity dispersion.*

The permittivity starts at a level determined by the water content in the emulsion. This permittivity decreases to the final level, which depends on the amount of hydrates formed. The permittivity spectrum of the emulsion at t=4 h differs from the permittivity spectrum obtained at t=18 h. This is due to a much lower content of free water in the emulsion while hydrate forming is almost complete.

The permittivity dispersion spectrum can be used to find the dielectric relaxation frequency due to the hydrate formation (See section 2.2.2). The permittivity spectra in Figure 5.4 do not give a complete picture of the permittivity dispersion. More measurements in the lower frequency range are needed in order to obtain a complete picture of the permittivity dispersion, and consequently, the relaxation frequency related to the hydrate formation.

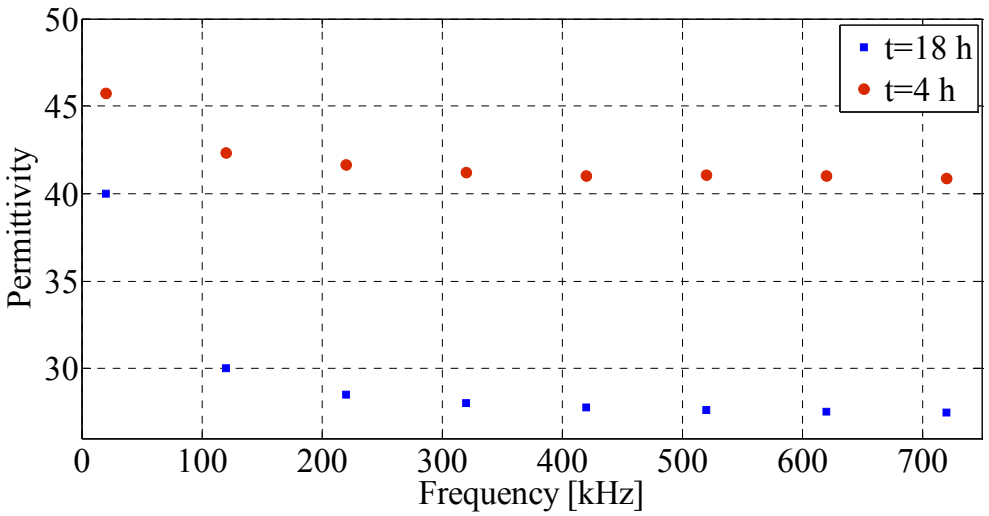

Figure 5.4: Permittivity spectra of the hydrate forming emulsion at t=18 h and t=4 h.

5.2. Permittivity measurements of oil continuous emulsion

The overall duration of the experiment for permittivity measurement of the oil continuous emulsion was much longer than the experiment performed with the water continuous emulsion. The reason for such prolonged experiment comes from the fact that firstly, hydrate formation phenomenon involves the interaction of free water molecules with Cyclopentane, and the chance for such interactions can be very low if there is a low amount of water in the sample. Secondly, as mentioned in Section 4.3, this experiment was commenced while the prepared oil continuous emulsion had been at the ambient temperature. Thus, it took a long time for the temperature of the emulsion to fall to the desired temperature of 3° C. In the rest of this section a thorough analysis of the experimental results is presented.

Figure 5.5 (a) and Figure 5.5 (b) show the capacitance and temperature data collected every 15 seconds over 160 hours for 8 different frequencies between 20 and 720 kHz. In Figure 5.5 (c), the permittivity data is shown. This figure is obtained by using the calibration curves of the capacitance sensor (Section 4.2.1). The temperature chamber controls the temperature of the experimental environment. However, for the purposes of visual observation, it was necessary to open and close the door of the chamber occasionally which led to instant changes in temperature over time. These unwanted changes in temperature may have affected the hydrate formation process and reflected on the permittivity variation. In order to be aware of the exact moment of any change in temperature due to opening/closing the chamber door, the inside temperature of the chamber was recorded. Figure 5.5 (d) shows the temperature variations inside the temperature chamber. The sharp peaks correspond to the moments the chamber door was opened.

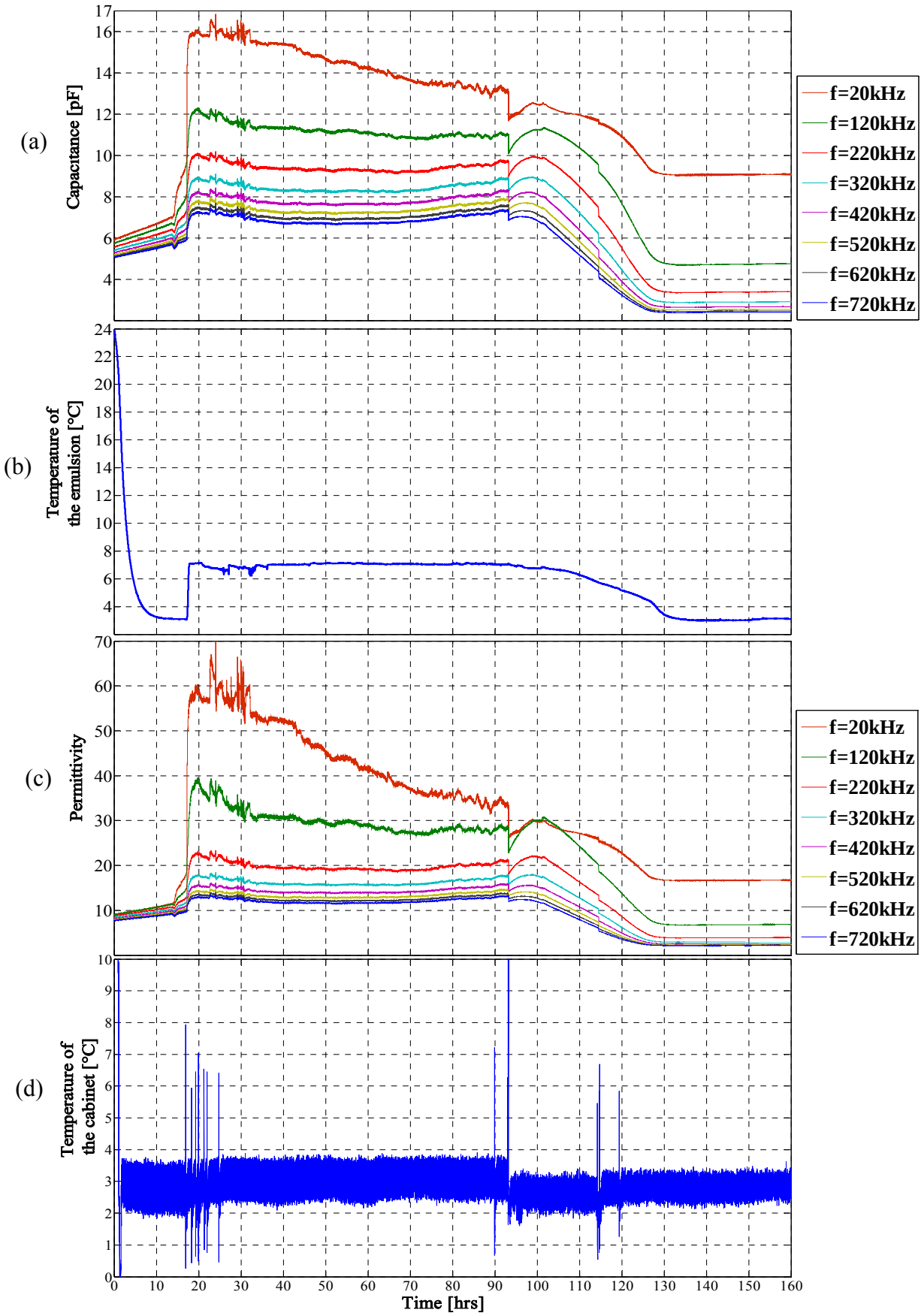

Figure 5.5: (a) Capacitance measurement as a function of time for 10 frequencies between 20 and 720 kHz. (b) Temperature history of the sample test. (c) Permittivity data as a function of time. (d) Temperature variation inside the temperature chamber.

In order to facilitate the interpretation of the results, they are divided into three phases with corresponding sub-figures:

- Pre hydrate formation phase: within the time frame of 0-17 h (Figure 5.6)
- Hydrate formation phase: within the time frame of 17-138 h (Figure 5.7)
- Post hydrate formation phase: within the time frame of 138-160 h (Figure 5.8)

In the following sections, each of these phases will be analyzed separately.

5.2.1. Pre hydrate formation phase

Figure 5.6 shows the measured permittivity and temperature of the hydrate forming emulsion, as the temperature of the emulsion is reduced from ambient to the chamber temperature of 3 °C.

It took approximately 10 h for the temperature of the emulsion to fall from ambient to 3 °C. During this period, it can be seen from Figure 5.6 (a) that the measured permittivity of the sample increases with time. This trend can be due to the fact that the permittivity of water has a temperature dependent nature. It is reported that in an oil-water emulsion, decreasing the temperature leads to an increases in the permittivity of water, while the permittivity of oil remains almost constant [87]. It is also probable that evaporation of Cyclopentane takes part in increasing the permittivity. Therefore, the water content of the emulsion may be raised, and this would lead to an increase in the permittivity of the emulsion as well.

To confirm the above statement, the volume fraction of water in the emulsion can be calculated at different times and compared to its initial value in the emulsion (β=40%). For this purpose, Bruggeman's theory of the effective permittivity of mixtures is used [88]. This can be used to calculate the overall permittivity of a dielectric mixture:

$$1-\beta=(\frac{\varepsilon_{eff}-\varepsilon_2}{\varepsilon_1-\varepsilon_2})(\frac{\varepsilon_1}{\varepsilon_{eff}})^{1/3} \quad (36)$$

Where β (or water cut) is the volume fraction of water in a water-in-oil mixture, $\varepsilon_1=\varepsilon_{oil}$ and $\varepsilon_2=\varepsilon_{water}$. In this model, assuming an ideal water-in-oil emulsion, all particles (water droplets) are assumed to be spheroid and distributed heterogeneously through the continuous phase (oil).

To calculate the volume fractions of water in the emulsion (β) during the first 10 hours (Equation (36)), 4 different points (ε_{eff}) from the permittivity curve at f=20 kHz were selected on Figure 5.6 (a), and the corresponding temperature values (T) were found from Figure 5.6 (b). To find the permittivity of water (ε_{water}) the following relation was used [87]:

$$\varepsilon_{water}=a\,exp[b(T-T_0)] \quad (37)$$

with $a=78.35, T_0=298.15\,\text{K}$ and $b=-4.55\times10^{-3}K^{-1}$, which describes the temperature dependent permittivity of water. Permittivity of Cyclopentane (ε_{oil}) was considered to be equal to 2. Therefore, using Equation (36), the volume fractions of water (β) were calculated (See Table 5.1).

Table 5.1: Calculated volume fractions of water (considering an oil continuous mixture) at 4 different times during the first 10 hours.

Time [h]	T [°C]	ε_{eff}	ε_{water}	ε_{oil}	β
1.83	15	9.25	81.99	2	45.4%
3.15	9	9.52	84.26	2	46%
6.78	4	10.14	86.20	2	47.4%
12.10	3	11.10	86.60	2	49.6%

Comparing the volume fractions of water during the first 10 hours (Table 5.1) to its initial value in the emulsion (β=40%) indicates that the increase in water in the emulsion can be due to the Cyclopentane evaporation phenomenon.

After the temperature of the emulsion became stabilized at 3 °C, the emulsion was left for approximately 4 hours to examine the possibility of hydrate formation without adding ice. During this period, the permittivity kept increasing which can be due to probable Cyclopentane evaporation. However, a permittivity drop at t=14.3 h can be noted. The reason for this permittivity change is likely to be related to the morphology of the hydrate forming mixture. The permittivity drop was followed by a higher rate increase. Such an increase can be due to probable inhomogeneities in the emulsion. The inhomogeneity can be due to the mixer malfunctioning, which can lead to the formation of water layers and measuring a higher permittivity, consequently.

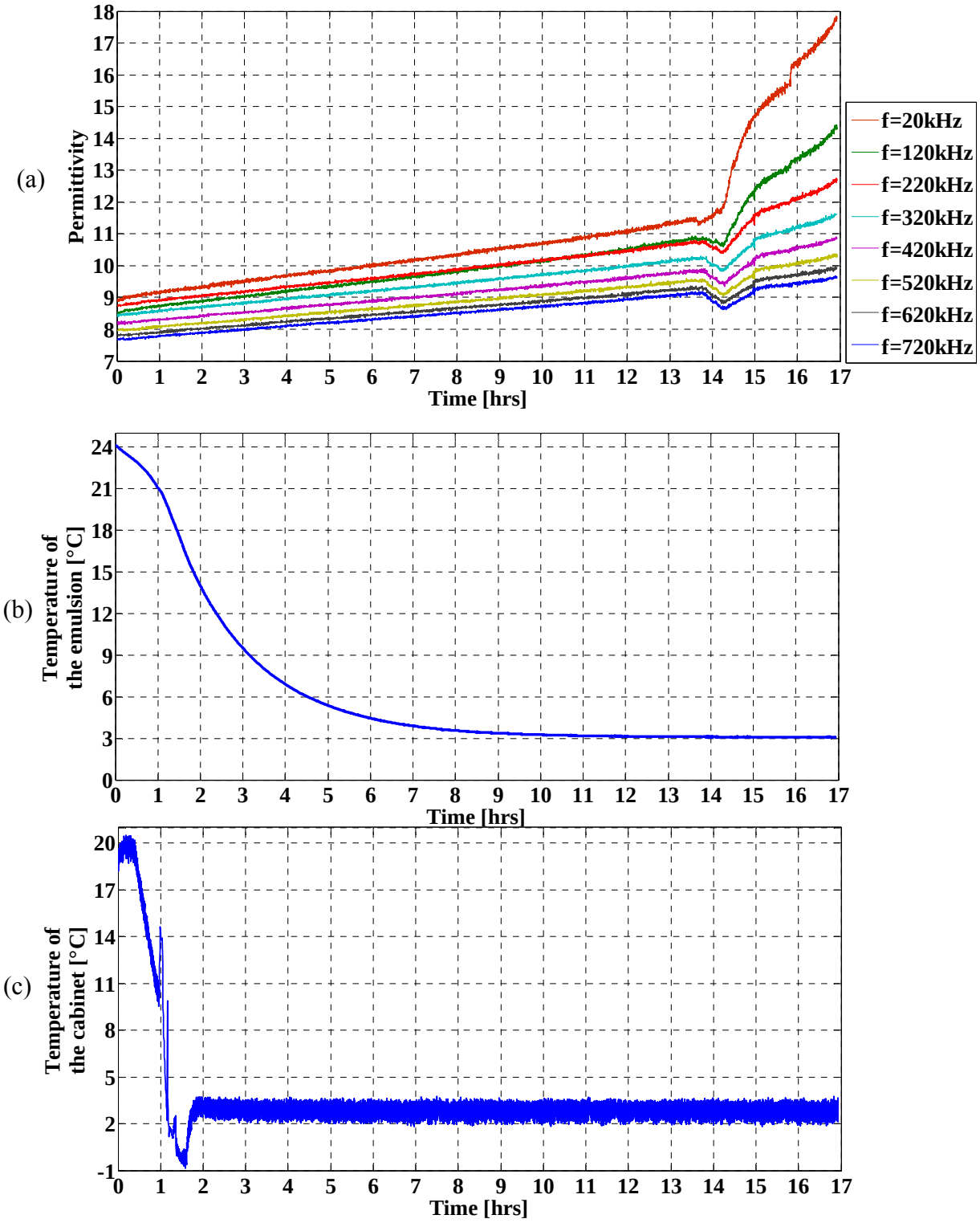

Figure 5.6 (a) Permittivity measurements of the emulsion before hydrate formation starts. (b) Temperature history of the emulsion. (c) Temperature changes inside the temperature chamber.

5.2.2. Hydrate formation phase

As pointed out in the previous section, the emulsion was left several hours to determine whether hydrate can form spontaneously. However, no evidence of hydrate formation was observed. Thus, to trigger hydrate formation, a small piece of ice was added to the emulsion at t=17 h. The first temperature peak in Figure 5.7 (c) is due to the opening of the temperature chamber door needed to add ice to the emulsion.

About 20 minutes after adding the ice, a sudden temperature increase of several degrees in the emulsion was observed (Figure 5.7 (b)) which is a typical indication of the onset of hydrate formation[7]. The temperature rise in the emulsion was accompanied by a corresponding significant increase in the measured permittivity of the emulsion (Figure 5.7 (a)). As the permittivity rise occurred at exactly the same time at which the temperature increased, it can be concluded that the capacitance sensor was measuring the permittivity changes due to the onset of hydrate formation in the emulsion. The reason for observing such a significant increase in permittivity can be due to a phase inversion[8] in the emulsion from the oil-continuous to the water-continuous phase. The phase inversion can be a consequence of morphological changes and rheological properties of the hydrate forming emulsion. Therefore, it is likely that the hydrate forming emulsion was no longer in the oil-continuous phase when the hydrate formation was started, and the attempt to perform hydrate permittivity measurements on an oil-continuous sample was likely to fail.

After the significant increase in the measured permittivity which might be caused by the phase inversion, a gradual permittivity decrease can be observed which is due to the fact that existing free water molecules in the emulsion become involved in the formation of hydrate. However, considerable fluctuations in the measured permittivity are observed at the outset of hydrate formation between 20 to 35 h. By visual observation of the emulsion, it was found that the homogeneous emulsion had turned into a mixture of liquid and slurry. It is likely that the mixer was having difficulty in mixing the slurry, and the homogeneous emulsion might have been occasionally turned into a layered emulsion, leaving the liquid containing water (continuous water phase) at the bottom and the formed

[7] The reason for temperature rise is from the exothermic nature of the hydrate formation reaction.
[8] The phase inversion phenomenon means that the dispersed phase (water) switches to the continuous phase.

hydrate together with the remaining Cyclopentane on the top (continuous oil phase). Therefore, the appearance of permittivity fluctuations can be correspondent to movement of the layers.

The overall decrease in the measured permittivity can be an indication of further hydrate formation. As long as there are free water molecules remained in the emulsion, the process of hydrate formation can continue. During this period, the temperature of the emulsion remains constant at 7 °C (the equilibrium temperature of Cyclopentane hydrate [78]) which can be seen in Figure 5.7 (b). By decreasing the number of free water molecules in the emulsion, which implies that the hydrate formation process is reaching to its final stage, the tendency of the temperature is to fall to the ambient temperature (T=3 °C). This is because once the hydrate formation process is complete, the heat release from the hydrate formation reaction stops. Thus, the temperature decrease can be considered as an indication of completing the hydrate formation process.

However, 75 hours after the onset of hydrate formation, no temperature drop was observed, and the resultant emulsion was still in a slurry state (Figure 5.10 (a)). This can indicate that in addition to the formed hydrate, there was still some water present. It was decided to remove the stirrer in order to let the emulsion form further hydrates. The decision was made due to the fact that the continuous running of the stirrer could have produced some heat, which could have caused a slight increase in the temperature, which could affect the hydrate formation process. Eventually, by removing the stirrer, the temperature of the emulsion showed a decrease from its equilibrium value.

At the moment of removing the stirrer, a sudden permittivity drop followed by an increase was observed. The sudden permittivity drop may be due to the removal of the stirrer. The reason for the permittivity increase may be due an increase in the water fraction of the slurry emulsion. It is likely that removing the stirrer could release some amount of water trapped beneath the slurry emulsion. The released water would then take part in further hydrate formation and result in a further decrease in permittivity.

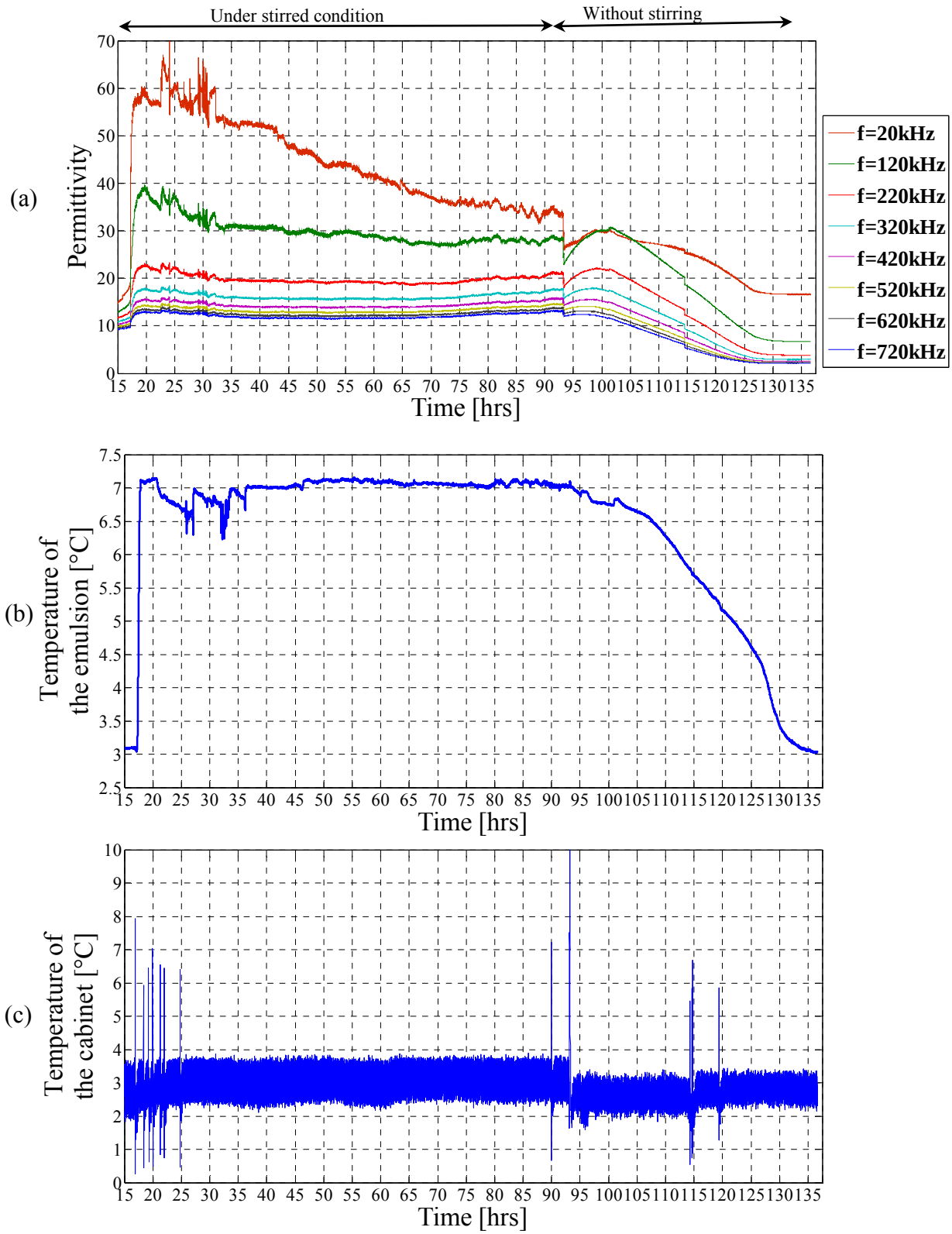

Figure 5.7: (a) Permittivity measurements of the emulsion during hydrate formation. (b) Temperature history of the emulsion. (c) Temperature changes inside the temperature chamber.

5.2.3. Post hydrate formation phase

At t=100 h, the permittivity began to decrease followed by a plateau which can indicate the completion of hydrate formation (Figure 5.8 (a)). Observing a constant value for permittivity along with measuring a constant value for temperature can be interpreted as the completion of the hydrate formation. At this time, the emulsion was most likely converted into pure hydrate observed as a hard solid substance (Figure 5.10 (b)).

It is reported that the permittivity of hydrate at f=20 kHz is approximately 43 [14]. However, the measured permittivity at the end of the experiment is approximately equal to 17. The reason for measuring a lower permittivity value may be due to the fact that after the 4 day experiment, a significant amount of the emulsion had evaporated, and the emulsion level had fallen below the sensor electrodes' upper edges, which was confirmed visually (See Figure 5.10 (b)).

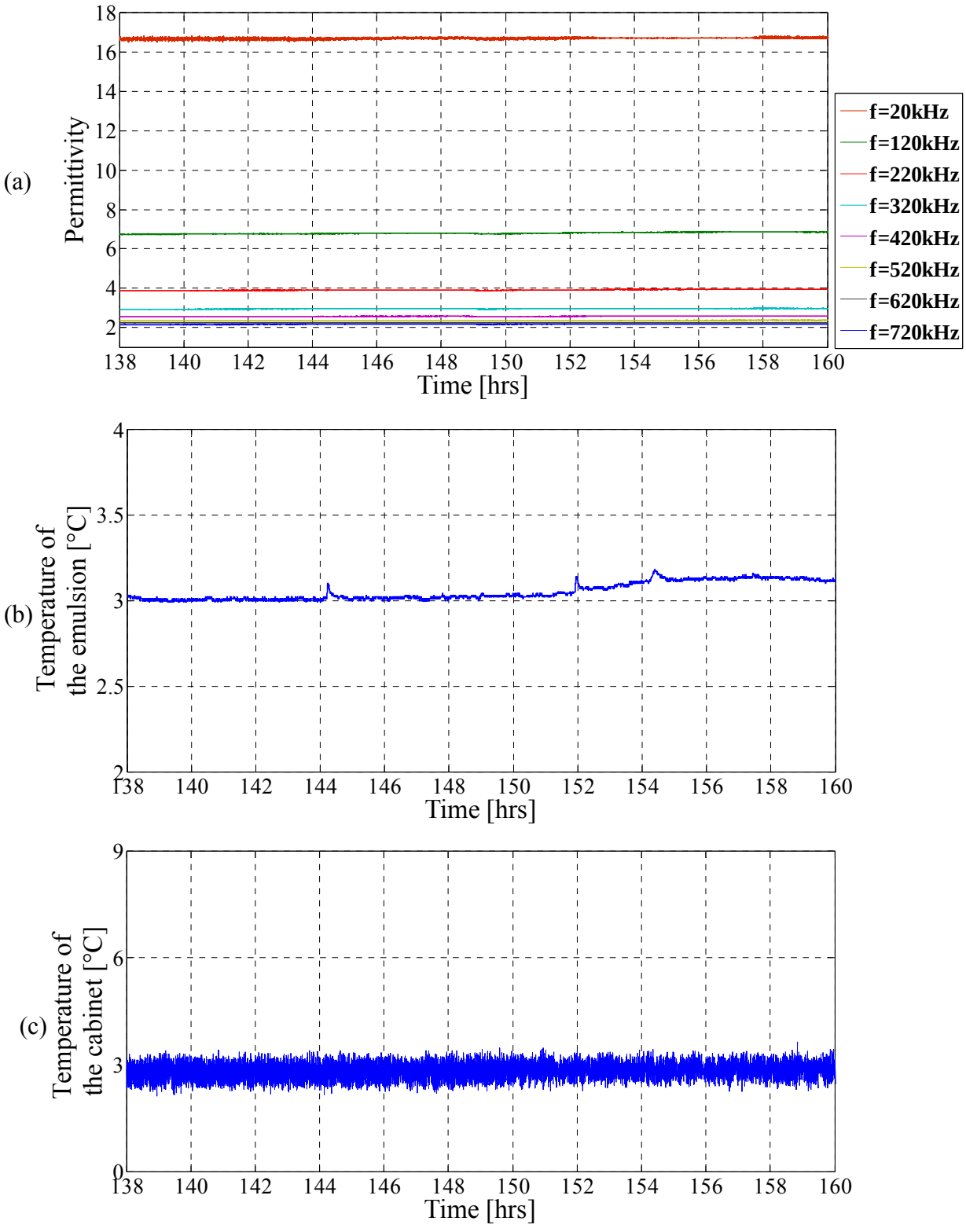

Figure 5.8: (a) Permittivity of the emulsion after hydrate formation is completed. (b) Temperature history of the emulsion. (c) Temperature variation inside the temperature chamber.

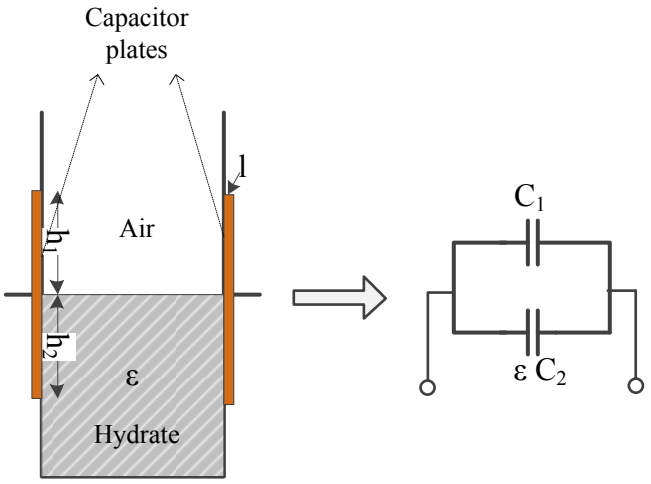

Figure 5.9: Equivalent circuit diagram of the capacitance sensor when the formed hydrate level is lowered to 50% of the electrodes' vertical length. The shaded area represents the formed hydrate layer with a permittivity ε value between 40 and 50.

The level of the emulsion was at about 50 % of the electrodes vertical length. This condition was used to estimate the capacitance measured by the sensor. To do so, the curved electrode capacitance sensor is approximated by a flat plate configuration as shown in Figure 5.9. The equivalent capacitance C_{meas} for such a configuration is equal to:

$$C_{meas} = C_1 + \varepsilon . C_2 \tag{38}$$

If C_{air} is the capacitance of a parallel plate air-filled capacitor of length h and width l, C_{meas} can be written as follows:

$$C_{air} = \varepsilon_0 \frac{A}{d} = \frac{h.l}{d} = \varepsilon_0 \frac{(h_1 + h_2).l}{d} \tag{39}$$

$$C_{meas} = \left(\frac{h - h_2 + \varepsilon . h_2}{h}\right) . C_{air} = [(\varepsilon - 1)\frac{h_2}{h} + 1] . C_{air} \tag{40}$$

Therefore, for $\frac{h_2}{h} = 0.5$, and $\varepsilon \sim 43$, the measured permittivity becomes:

$$\varepsilon_{meas} = (\varepsilon - 1)\frac{h_2}{h} + 1 = 21 \tag{41}$$

By comparing the estimated permittivity ε_{meas} (i.e 21) with the final measured permittivity value of the emulsion which is equal to 17, it can be concluded that the substance left after the end of the experiment might be pure hydrate.

Figure 5.10: (a) Cyclopentane hydrate after removing the mixer. (b) Pure Cyclopentane hydrate at the end of the experiment.

In Figure 5.11 the permittivity spectra of the emulsion are plotted for three different times regarding to pre hydrate formation (t=6 h), during hydrate formation (t=43 h) and post hydrate formation (t=150 h). At t=6 h, when the hydrate formation is not started, the permittivity spectrum shows a slight change. At t=43 h and t=150 h, the permittivity dispersion due to the hydrate formation are clearly seen. Observing a difference between the permittivity spectra is due to a lower content of free water caused by the hydrate formation.

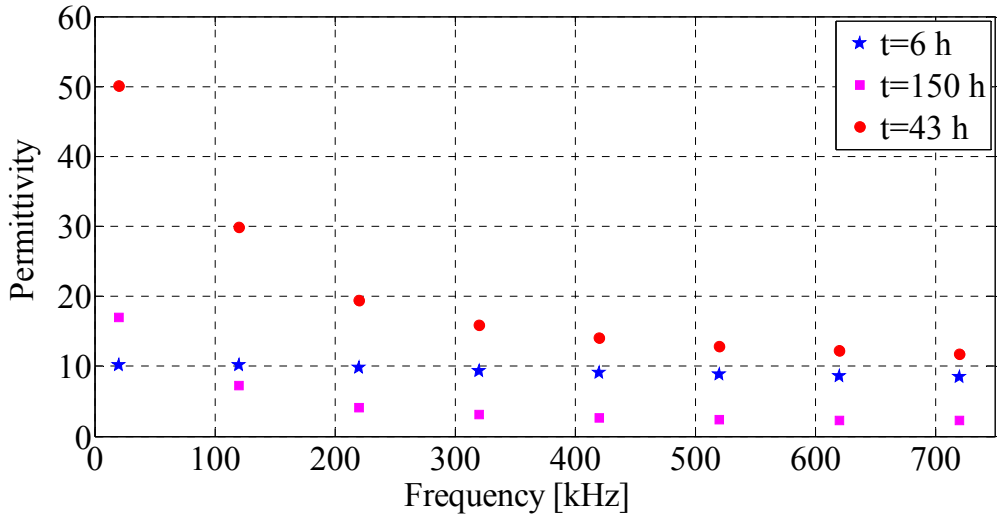

Figure 5.11: Permittivity spectra of the hydrate forming emulsion at t=6 h, t=43 h and t=150 h.

6. Conclusion

The objective of this thesis was to conduct a feasibility study on a permittivity measurement system based on the capacitance sensing technique for monitoring of gas hydrate formation. It was shown that formation of gas hydrates in emulsions can be monitored using capacitance measurement sensors.

The thesis gives an introduction to the gas hydrate issue; the techniques in use or under evaluation for dealing with this issue, and the potential applicability of the capacitance sensors for monitoring gas hydrates has been explained. This is followed by the required insight into the fundamentals of the gas hydrate formation phenomenon together with the fundamental principles of capacitance sensors. The modeling of a capacitance sensor was discussed with the aim of finding an appropriate sensor configuration, which was used to construct a prototype sensor setup for the purpose of permittivity measurement experiments under varying operating conditions.

The experimental procedures for the permittivity measurements of two hydrate-forming samples with different water fractions in the kHz frequency range were explained. It should be noted that these experiments were being conducted for the first time. The measurement results along with their analysis were investigated accordingly.

The measurement analysis revealed that the capacitance sensor is able to identify several of process states occurring during the hydrate generation process. The derived information can indicate (i) the time at which the onset and completion of hydrate formation occurs, (ii) the volume fraction of water, (iii) the probable occurrence of phase inversion in the multiphase hydrate-forming sample, and (iv) the permittivity relaxation due to the hydrate formation. Consequently, it can be claimed that monitoring of the hydrate generation in multiphase hydrocarbon flow using capacitance sensors is a feasible proposition. However, there are still some issues that need to be investigated further. In addition, it is unclear to what extent we will be able to distinguish the detected parameters related to the hydrate generation from other phenomena that might happen during hydrate formation. In

order to correlate the hydrate formation phenomena occurring during the formation process, additional experiments must be carried out.

7. Further work

The capacitance sensor has the potential for use both relating to fundamental studies of hydrate characterization in the laboratory and for on-line gas hydrate monitoring. There are, however, several potential improvements that could be considered.

The following areas require further investigation in order to progress the use of the capacitance measurements systems for studies of gas hydrate in the laboratory:

- More knowledge about the hydrate crystal morphology and agglomerating behavior is desirable.
- More hydrate-forming samples should be examined.
- Use of a time-lapse video camera assembly to record and monitor the changes during formation of gas hydrates.
- Examine oil-continuous samples with varying salinity of the water phase.
- Investigate the effect of the stirring rate.
- Use a more efficient mixer in order to produce improved long-lasting homogeneous mixtures.

Further developments are necessary before the capacitance sensor system can be used as an on-line monitoring system for the detection of gas hydrates in multiphase flows e.g. installed on sub-sea pipelines. Along with necessary work on correlating the permittivity changes to the hydrate generation process, the following issues need to be addressed:

- The sensor needs to be mounted on a laboratory flow-loop where on-line tests of realistic flow conditions can be performed. In this loop, factors critical to on-line systems can be studied under controlled conditions. These factors include the effect of scaling and fouling of the sensors and the long-time effect of small variations in temperature, pressure and vibration.
- More realistic samples like the pressurized crude oil samples should be examined.

- The capacitance sensor must be capable of withstanding the hostile subsea environment by being stabile, have a long lifetime, and be able to sustain extreme pressure and temperature conditions.
- Instead of using the impedance analyzer, a low-noise electronic measurement system applicable for on-line use must be designed.
- In the subsea environment, the flow regimes in the production pipes can differ significantly from that of the ideal homogeneous mixture, and in-line mixers are deemed unwanted due to pressure loss and maintenance costs. Therefore, it is essential to find a practical solution to make the sensor less flow regime dependent. A suggested solution is to design and employ helical shaped surface plate electrodes, based on 180° twisted electrostatic field or rotating electric fields [59-61].
- Considering multi-phase hydrocarbon flow as the dielectric sample under test, the performance of the capacitance sensors is limited to the measurements of gas/oil-continuous mixtures. These techniques also have potential for monitoring gas hydrate formation in wet gas[9] wells.

[9] The term "wet gas" is used for processes where the proportion of liquid phase is no greater than about 5%

References

1. E.D. Sloan, *Gas Hydrates: Review of Physical/Chemical Properties,* Energy & Fuels, vol. 12, no. 2, pp. 191-196, 1998.

2. P. Englezos, *Clathrate hydrates,* Industrial & Engineering Chemistry Research, vol. 32, no. 7, pp. 1251-1274, 1993.

3. T.R. Lin, B. Guo, S. Song, A. Ghalambor, J. Chacko, *Offshore pipelines*, Gulf Professional Publishing, ISBN 075067847X, 2005.

4. S.K. Kelkar, M.S. Selim, E.D. Sloan, *Hydrate dissociation rates in pipelines,* Fluid Phase Equilibria, vol. 150–151, pp. 371-382, 1998.

5. Y.F. Makogon, *Hydrates of Hydrocarbons*, Pennwell Books, ISBN 0878147187, 1997.

6. B. Tohidi, SPE, A. Chapoy, J. Yang, Heriot-Watt University, *Developing Hydrate Monitoring and Early Warning Systems*, SPE Projects, Facilities & Construction, vol. 4, no. 1, pp. 1-6, 2009

7. E.D. Sloan, *Fundamental principles and applications of natural gas hydrates,* Nature, vol 426, no. 6964, pp. 353-363, 2003.

8. A.R. Von Hippel, *Dielectric Materials and Applications,*Wiley, New York, ISBN 1580531237, 1954.

9. T.J. Buchanan, *Balance methods for the measurement of permittivity in the microwave region,* Proceedings of the IEE - Part III: Radio and Communication Engineering, vol. 99, no. 58, pp. 61-66, 1952.

10. U. Kaatze, R. Pottel, and A. Wallusch, *A new automated waveguide system for the precise measurement of complex permittivity of low-to-high-loss liquids at microwave frequencies,* Measurement Science and Technology, vol. 6, no. 8, paper 1201, 1995.

11. L. Zanforlin, *Permittivity Measurements of Lossy Liquids at Millimeter-Wave Frequencies,* Microwave Theory and Techniques, IEEE Transactions on, vol. 31, no. 5, pp. 417-419, 1983.

12. T. Jakobsen, J. Sjöblom, and P. Ruoff, *Kinetics of gas hydrate formation in w/o-emulsions the model system trichlorofluoromethane/water/non-ionic surfactant studied by means of dielectric spectroscopy,* Colloids and Surfaces A: Physicochemical and Engineering Aspects, vol. 112, no. 1, pp. 73-84, 1996.

13. K. Folgerø, *Coaxial Sensors for Broad-band Complex Permittivity Measurements of Petroleum Fluids*, PhD thesis, Department of Physics, University of Bergen, 1997.

14. T. Jakobsen, K. Folgerø, *Dielectric measurements of gas hydrate formation in water-in-oil emulsions using open-ended coaxial probes,* Measurement Science and Technology, vol. 8, no. 9, pp. 1006-1015, 1997.

15. F. Rauh, B. Mizaikoff, *Spectroscopic methods in gas hydrate research.* Analytical and bioanalytical chemistry, vol. 402, no.1, pp. 163-173, 2012.

16. E.D. Sloan, *Physical/chemical properties of gas hydrates and application to world margin stability and climatic change,* Geological Society, London, Special Publications, vol. 137, no. 1, pp. 31-50, 1998.

17. E.D. Sloan, C.A. Koh, *Clathrate hydrates of natural gases*, CRC Press, 3rd edition, ISBN 0849390788, 2008.

18. S.Y. Lee, G.D. Holder, *Methane hydrates potential as a future energy source.* Fuel Processing Technology, vol. 71, no. 1–3, pp. 181-186, 2001.

19. J. Gudmundsson, A. Borrehaug. *Frozen hydrate for transport of natural gas*. Proceedings of 2nd International Conference on Gas Hydrate, Toulouse, France, 1996.

20. J.S. Gudmundsson, M. Mork, O.F. Graff, *Hydrate non-pipeline technology*, Proceedings of 4th International Conference on Gas Hydrates, *Yokohama, Japan,* 2002.

21. H. Kaneko, *Natural gas transportation by methane hydrate,* Techno Mar, no. 842, pp. 586-594, 1999.

22. K.A. Kvenvolden, *Methane hydrates and global climate,* Global Biogeochemical Cycles, Vol. 2, no. 3, pp. 221-229, 1988.

23. J.P. Kennett, *Methane Hydrates in Quaternary Climate Change: The Clathrate Gun Hypothesis*, American Ceophysical Union, Washington DC, ISBN 0875902960, 2013.

24. D. Corak, T. Barth, S. Hoiland, T. Skodvin, C. Brekken, T. Sketne, *The Ecowat process for purification of water offshore: fundamental studies related to optimal operating conditions,* Proceedings of 21st International Oil Field Chemistry Simposium, Geilo, Norway, 2010.

25. A.M. Aliev, R.Y. Yusifov, A.R. Kuliev, Y.G. Yusifov, *Method of gas hydrate formation for evaluation of water desalination,* Russian Journal of Applied Chemistry, vol 81, no. 4, pp. 588-591, 2008.

26. L.K. Baxter, *Capacitive Sensors: Design and Applications*, John Wiley & Sons, ISBN 078035351X, 1996.

27. J.R. Reitz, F.J. Milford, R.W. Christy, *Foundations of electromagnetic theory*, 4th edition, Addison-Wesley, ISBN 0321581741, 2008.

28. K.S. Cole, R.H. Cole, *Dispersion and absorption in dielectrics I, Alternating current characteristics,* The Journal of Chemical Physics, Vol. 9, no. 4, 1941.

29. N.E. Hill, W.E. Vaughan, A.H. Price, M. Davis, *Dielectric properties and molecular behaviour*, Van Nostrand Reinhold Inc., U.S., ISBN 0442034113, 1969.

30. R. Puers, *Capacitive sensors: When and how to use them*, Sensors and Actuators A: Physical, vol. 37–38, pp. 93-105, 1993.

31. R.V. Jones, J.C.S. Richards, *The design and some applications of sensitive capacitance micrometers.* Journal of Physics E: Scientific Instruments, vol. 6, no. 7, 1973.

32. A. Fertner, A. Sjolund, *Analysis of the performance of the capacitive displacement transducer.* Instrumentation and Measurement, IEEE Transactions on, vol. 38, no. 4, pp. 870-875, 1989.

33. M. Kim, W. Moon, E. Yoon, K.R. Lee, *A new capacitive displacement sensor with high accuracy and long-range,* Sensors and Actuators A: Physical, vol. 130–131, pp. 135-141, 2006.

34. C. Tianming, N. Bowler, *Analysis of a concentric coplanar capacitive sensor for nondestructive evaluation of multi-layered dielectric structures,* Dielectrics and Electrical Insulation, IEEE Transactions on, vol. 17, no. 4, pp. 1307-1318, 2010.

35. A.V. Mamishev, K. Sundara-Rajan, F. Yang, Y. Du, M. Zahn, *Interdigital sensors and transducers,* Proceedings of the IEEE, vol. 92, no. 5, pp. 808-845, 2004.

36. C. Tianming, N. Bowler, J.R. Bowler, *Analysis of Arc-Electrode Capacitive Sensors for Characterization of Dielectric Cylindrical Rods,* Instrumentation and Measurement, IEEE Transactions on, vol. 61, no. 1, pp. 233-240, 2012.

37. T. Chen, N. Bowler, *A rotationally-invariant capacitive probe for materials characterisation,* Materials Evaluation, vol. 70, pp. 161-172, 2012.

38. L. Gu, Q.A. Huang, M. Qin, *A novel capacitive-type humidity sensor using CMOS fabrication technology,* Sensors and Actuators B: Chemical, vol. 99, no. 2–3, pp. 491-498, 2004.

39. M.C. Zaretsky, L. Mouayad, J.R. Melcher, *Continuum properties from interdigital electrode dielectrometry,* Electrical Insulation, IEEE Transactions on, vol. 23, no. 6, pp. 897-917, 1988.

40. F. Lisdat, D. Schäfer, *The use of electrochemical impedance spectroscopy for biosensing.* Analytical and Bioanalytical Chemistry, vol. 391, no. 5, pp. 1555-1567, 2008.

41. P.J. Shull, A.V. Clark, P.R. Heyliger, J.C. Moulder, B.A. Auld, *Characterization of capacitive array for NDE applications,* Research in Nondestructive Evaluation, vol 2, no. 1, pp. 11-27, 1990.

42. J.R. Matey, J. Blanc, *Scanning Capacitance Microscopy,* Applied Physics, vol. 57, no. 1437 pp. 110-117, 1985.

43. I.C. Shay, M. Zahn, *Cylindrical geometry electroquasistatic dielectrometry sensors,* Dielectrics and Electrical Insulation, IEEE Transactions on, vol. 12, no. 1, pp. 41-49, 2005.

44. A.A. Nassr, W.H. Ahmed, W.W. El-Dakhakhni, *Coplanar capacitance sensors for detecting water intrusion in composite structures,* Measurement Science and Technology, vol. 19, no. 7, pp. 075702, 2008.

45. A.A. Nassr, W.W. El-Dakhakhni, *Non-destructive evaluation of laminated composite plates using dielectrometry sensors,* Smart Materials and Structures, vol. 18, no. 5, pp. 055014, 2009.

46. P. Linderholm, J. Vannod, Y. Barrandon, F. Renaud, *Bipolar resistivity profiling of 3D tissue culture,* Biosensors and Bioelectronics, vol. 22, no. 6, pp. 789-796, 2007.

47. W.Q. Yang, L. Peng, *Image reconstruction algorithms for electrical capacitance tomography,* Measurement Science and Technology, vol. 14, no. 1, 2003.

48. D. Xie, Z. Huang, H. Ji, H. Li., *An Online Flow Pattern Identification System for Gas–Oil Two-Phase Flow Using Electrical Capacitance Tomography,* Instrumentation and Measurement, IEEE Transactions on, vol 55, no. 5, pp. 1833-1838, 2006.

49. A.E. Corlett, *Three-phase Flow Pattern Recognition in Horizontal Pipelines using Electrical Capacitance Tomography,* Journal of Visualization, vol. 2, no 1, p. 31-36, 1999.

50. W.C. Heerens, *Application of capacitance techniques in sensor design,* Journal of Physics E: Scientific Instruments, vol. 19, no. 11, pp. 897, 1986.

51. W.H. Ahmed, *Capacitance Sensors for Void-Fraction Measurements and Flow-Pattern Identification in Air–Oil Two-Phase Flow,* Sensors Journal, IEEE, Vol. 6, no. 5, pp. 1153-1163, 2006.

52. D. Lowe, K.S. Rezkallah, *A capacitance sensor for the characterization of microgravity two-phase liquid-gas flows,* Measurement Science and Technology, vol. 10, no. 10, pp. 965, 1999.

53. M. Merilo, R. Dechene, W. Cichowlas, *Void fraction measurement with a rotating electric field conductance gauge,* Journal of Heat Transfer, vol 99, pp. 330-332, 1977.

54. E.A. Hammer, *Three-component flow measurement in oil/gas/water mixtures using capacitance transducers, PhD thesis*, University of Manchester, Institute of Science and Technology, 1983.

55. R.B. Schuller, B. Engebretsen, M. Halleraker, *Measurement of water concentration in oil/water dispersions by a single-electrode capacitance probe*, Instrumentation and Measurement, IEEE Transactions on, vol. 53, no. 5, pp. 1378-1383, 2004.

56. J.J.M. Geraets, J.C. Borst, *A capacitance sensor for two-phase void fraction measurement and flow pattern identification,* International Journal of Multiphase Flow, vol. 14, no. 3, pp. 305-320, 1988.

57. W. Yang, Y. Li, Z. Wu, D. Tsamakis, C.G. Xie, S. Huang, C. Lenn, D. Learmonth, A. Culter, *Multiphase flow measurement by electrical capacitance tomography*, *Imaging Systems and Techniques (IST),* IEEE International Conference on, Penang, Malaysia 2011.

58. W. Managan, R. Doering, *Capacitive Transducers for Mass Flow Measurement, An Overview*, Proceedings of the Symposium on Instrumentation and Control for Fossil Energy Processes, ANL*,* 1979.

59. E.A. Hammer, J. Tollefsen, K. Olsvik, *Capacitance transducers for non-intrusive measurement of water in crude oil,* Flow Measurement and Instrumentation, Vol. 1, no. 1, pp. 51-58, 1989.

60. J. Ye, L. Peng, W. Wang, W. Zhou, *Optimization of Helical Capacitance Sensor for Void Fraction Measurement of Gas-Liquid Two-Phase Flow in a Small Diameter Tube,* Sensors Journal, IEEE, vol. 11, no. 10, pp. 2189-2196, 2011.

61. S.A. Tjugum, C. Sætre, G.A. Johansen. *Multibeam gamma-ray measurements and electrical tomography for improved multiphase flow metering*, Proceedimgs of the North Sea Flow Measurement Workshop, Tønsberg, Norway, 2011.

62. K. Umashankar, *Introduction to Engineering Electromagnetic Fields*, World Scientific, ISBN 9971509210, 1989.

63. S.S. Rao, *The Finite Element Method in Engineering*, Elsevier Science, ISBN: 9780750678285, 2010.

64. www.comsol.com, Multiphysics C., Comsol Multiphysics Inc., Burlington, MA, 1994.

65. Multiphysics C., *Introduction to Comsol Multiphysics®,* 2011.

66. *Comsol Multiphysics,* AC/DC Module User's Guide, 2012.

67. R. Fitzpatrick, *Maxwells Equations and the Principles of Electromagnetism*, Infinity Science Press, ISBN 1934015202, 2008.

68. V.V. Sarwate, *Electromagnetic Fields And Waves*, Bohem Press, ISBN 8122404685, 1993.

69. N Flores, Á Kuri-Morales, C Gamio, *An Application of Neural Networks for Image Reconstruction in Electrical Capacitance Tomography Applied to Oil Industry*, Progress in Pattern Recognition, Image Analysis and Applications, vol. 4225, pp. 371-380, 2006.

70. K.J. Alme, S. Mylvaganam, *Electrical Capacitance Tomography; Sensor Models, Design, Simulations, and Experimental Verification,* Sensors Journal, IEEE, vol. 6, no. 5, pp. 1256-1266, 2006.

71. D.R. DLide, *CRC Handbook of Chemistry and Physics: A Ready-reference Book of Chemical and Physical Data*, CRC PressI Llc, CRC Press, ISBN 0849304857, 2004.

72. P. Petong, R. Pottel, U. Kaatze, *Water−Ethanol Mixtures at Different Compositions and Temperatures. A Dieletric Relaxation Study,* The Journal of Physical Chemistry A, vol 104, no. 32, pp. 7420-7428, 2000.

73. A. Pramanik, *Electro-Magnetism: Theory and Applications*, PHI Learning Pvt. Ltd, ISBN 8120319575, 2004.

74. L. Peng, C. Mou, D. Yao, B. Zhang, D. Xiao, *Determination of the optimal axial length of the electrode in an electrical capacitance tomography sensor*, Flow Measurement and Instrumentation, vol. 16, no. 2–3, pp. 169-175, 2005.

75. T. Chen, N. Bowler, *Analysis of a capacitive sensor for the evaluation of circular cylinders with a conductive core*, Measurement Science and Technology, vol. 23, no. 4, 2012.

76. W.Q. Yang, *Modelling of capacitance tomography sensors*, Science, Measurement and Technology, IEE Proceedings, vol. 144, no. 5, pp. 203-208, 1997.

77. W.Q. Yang, T.A. York, *New AC-based capacitance tomography system,* Science, Measurement and Technology, IEE Proceedings, vol. 146, no. 1, pp. 47-53, 1999.

78. Nakajima, M., R. Ohmura, and Y.H. Mori, *Clathrate Hydrate Formation from Cyclopentane-in-Water Emulsions,* Industrial & Engineering Chemistry Research, vol 47 no. 22, pp. 8933-8939, 2008.

79. J. Zhang, J.W. Lee, *Inhibition Effect of Surfactants on CO2 Enclathration with Cyclopentane in an Unstirred Batch Reactor*, Industrial & Engineering Chemistry Research, vol. 48, no. 10, pp. 4703-4709, 2009.

80. E.D. Sloan, *Hydrate Engineering*, Society of Petroleum Engineers (U.S.), ISBN 1555630871, 2000.

81. E.G. Dirdal, C. Arulanantham, H. Sefidroodi, M. A. Kelland, *Can cyclopentane hydrate formation be used to rank the performance of kinetic hydrate inhibitors?,* Chemical Engineering Science, vol. 82, pp. 177-184, 2012.

82. P.U. Karanjkar, J.W. Lee, J.F. Morris, *Calorimetric investigation of cyclopentane hydrate formation in an emulsion*, Chemical Engineering Science, vol. 68, no. 1, pp. 481-491, 2012.

83. C.J. Brown, X. Ni, *Evaluation of rate of cyclopentane hydrate formation in an oscillatory baffled column using laser induced fluorescence and energy balance*, Chemical Engineering Journal, vol. 157, no. 1, pp. 131-139, 2010.

84. M.A. Kelland, *History of the Development of Low Dosage Hydrate Inhibitors*, Energy & Fuels, vol. 20**,** no. 3, pp. 825-847, 2006.

85. S.M. Huang, R.G. Green, A.B. Plaskowski, M.S. Beck, *Conductivity effects on capacitance measurements of two-component fluids using the charge transfer metho*d. Journal of Physics E: Scientific Instruments, vol. 21, no. 6, 1988.

86. P. Wang, A. Anderko, *Computation of dielectric constants of solvent mixtures and electrolyte solutions,* Fluid Phase Equilibria, vol. 186, no. 1–2, pp. 103-122, 2001.

87. U. Kaatze, *Reference liquids for the calibration of dielectric sensors and measurement instruments,* Measurement Science and Technology, vol. 18, no. 4, 2007.

88. D.A.G. Bruggeman, *Berechnung verschiedener physikalischer konstanten von heterogenen substanzen, i. dielektrizitätskonstanten und leitfähigkeiten der mischkörper aus isotropen substanzen*, Annalen der Physik, vo. 416, no. 7, pp. 636–664, 1935.